Study on Condition Monitoring and Diagnosis Method of Rotating Machinery – Vibration Mechanism Clarification and Intelligent Diagnosis Method for Structural Fault of Rotating Machinery

（回転機械設備の状態監視･診断法に関する研究 －構造系異常振動のメカニズム解明と知的診断法－）

三重大学大学院　生物資源学研究科

共生環境学専攻　環境・生産科学講座

環境情報システム工学教育研究分野

学籍番号　516D201

学生氏名　関照議

指導教員　陳山　鵬　教授

Content

1. Abstract

In order to effectively detect and identify the structure faults of rotating machinery, especially the precise diagnosis of structure faults at low speeds, in this study, we first proposed two kinds of dynamic model for shaft misalignment of rotating machinery as an entry point, the models will be used for vibration analysis of shaft misalignment state.

Subsequently, we proposed a new kind of dedicated symptom parameters for structure faults of rotating machinery. Based on these symptom parameters, fault diagnosis method for structure faults of rotating machinery by multi-positional and multi-directional signals fusion and sequential successive multivariate analysis can be realized. The method can realize the detection and type discrimination of structure faults.

Finally, we propose a precision diagnosis method that combines signal processing method which used empirical mode decomposition and sample entropy, with deep belief neural network (DBN). The advantage of this method is that the empirical signal decomposition method can be used to decompose the diagnosed signal into a plurality of intrinsic mode functions with high Signal to noise ratio (SNR), and then use the sample entropy as a criterion to screen the signals which containing a large amount of fault information. The screened signal are reconstructed into a new vibration signal. At last, the vibration signal is classified (precise diagnosis) by the deep learning method (DBN) which has strong pattern recognition function in the field of pattern recognition. The method has higher diagnostic precision than conventional methods. According to the experimental data measured by the rotating machinery in the abnormal states of each structure faults, the effectiveness of each method will be verified.

2. Introduction

Rotating machinery covers a broad range of mechanical equipment and plays a significant role in industrial applications. It generally operates under tough working environment and is therefore subject to faults [1]. It is very important to ensure that the large rotating machinery operates safely and reliably [2]. Misalignment is one of the most commonly observed faults in rotating machines [3]. The shaft misalignment state is often occurring in rotating machineries. Because it causes bad vibration and shortens the life of parts installed on the shaft, such as bearing, gear, etc. For example fault diagnosis of a motor system is inseparably related to the diagnosis of the bearing assembly [4]. Early detection and identification of misalignment type are very important to ensure the machine safety and production quality. Major economic benefits come from being able to predict with reasonable certainty how much longer a machine can safely operate (often a matter of several months from when incipient faults are first detected [5].

Vibration monitoring is one of the primary techniques of condition monitoring of rotating machine [6]. If a problem does occur the source of the problem is quickly identified and corrected. With proper knowledge and diagnostic procedures, it is normally possible to quickly pinpoint the cause of the vibration [7]. Current methods for predicting rotating machinery failures are summaried and classified as conventional reliability models, condition-based prognostics models and models integrating reliability and prognostics [8]. However, up to now, since the mechanisms of the abnormal vibration caused by shaft misalignment and the feature of vibration signal measured for diagnosis have not been made clear by theory yet, the diagnosis of the shaft misalignment in real plant is merely carried out by experience and statistical method. The accuracy of detecting and distinguishing shaft misalignment state is not enough high.

The health analysis of rotating machines can be assured by permanent condition monitoring systems. However, to satisfy the main requirements of predictive

maintenance, protective and condition monitoring techniques should be integrated with diagnostic methods aimed to identify the machine faults [9]. In order to clarify the vibration feature of shaft misalignment, in this paper, we establish dynamic models of misalignment states called "angle misalignment (see Fig. 1 (a))" and "offset misalignment (see Fig. 1 (b))" for vibration analysis to investigate the dynamic characteristics of shaft misalignment state. To verify the efficiency of the dynamic analysis proposed in this paper, we compare the results of computer simulations with experiments.

Because the vertical vibration caused by shaft misalignment states is affected by various conditions of the rotating shaft construction, it is difficult to establish a universal vibration model. The vibration in the axial direction is relatively easy to modeling universally. The basic reason of establishing the dynamic model in axial direction for misalignment state is that the forced vibration is mainly caused by the displacement of shaft coupling in axial direction when rotating, and the feature of vibration signal in vertical and axial direction are similar in shape, in other words the feature of respective spectra are basically similar. This fact is also proofed by real measurement of vibration signal in the misalignment state. Therefore, clarifying the feature of axial vibration by the analysis of the dynamic model in in axial direction can also basically explain the characteristics of the vibration in the vertical vibration for diagnosing the misalignment state. Traditional vibration analysis rules used in practical predictive maintenance to diagnose shaft misalignment are evaluated [10]. Misalignment state has two types called “angle misalignment” and “offset misalignment” as shown in Fig. 1 (a) and (b).

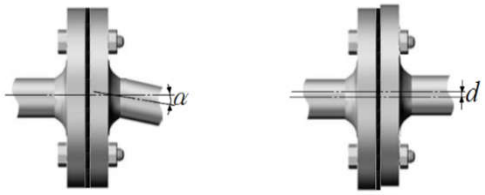

(a) (b)

Fig. 1 Misalignment states of rotating shaft ((a) Angular misalignment (b) Offset misalignment)

The structural faults of the rotating machine include those caused by such

mechanical structural defects as unbalance, misalignment, and loosening of the fasteners, resulting in abnormal vibration at a relatively low frequency. As the most common faults in rotating machinery, structural faults not only have direct adverse effects on the performance of the equipment and the quality of the product, but also cause excessive stress on the peripheral components such as bearings and gears, leading to secondary faults. This makes it extremely vital to realize that fault detection and type identification of structure faults states are very important to ensure machine safety and production quality [11, 12].

Compared to the normal state, the most common feature of the structural faults is the changes of the spectrum of vibration signal in the rotational frequency and its harmonic components. Although some studies have revealed part of spectral characteristics of a series anomalous state, it is still insufficient to accurately draw a distinguishing line between different structural faults [13]. In view of this, it is often very difficult to determine the anomaly types (precision diagnosis), especially an effective automatic diagnosis method has not yet been established in the diagnostic system. When the intelligent condition diagnostic system is developed via computer algorithms, the symptom parameters are required to express the characteristics of the vibration signal measured to distinguish the states of the machinery. Nonetheless, in the computer-based automatic diagnosis, especially at the early stage of structural faults, the noise of the measured vibration signal is very strong, therefore the anomaly identification sensitivity of symptom parameters commonly used in statistics (kurtosis, skewness, wave height, etc.) has remained low for long time. In other words, it would be difficult to detect the anomalies and distinguish their types by using these commonly used symptom parameters. Furthermore, as the automatic detection method of the structural faults based on conventional neural network is affected by noise, the data learned are fuzzy. Consequently, the learning by the neural network often cannot ensure the convergence, resulting in many difficulties in building a practical diagnosis system.

Currently dimensional or non-dimensional symptom parameters are widely used for fault diagnosis such as abnormal of centrifugal pump, rolling element bearing and

so on [14, 15]. Therefore, to effectively and automatically detect and identify the structural faults that may be present with the rotating machine, this research has proposed new symptom parameters (hereinafter referred to as the Structural Feature Symptom Parameter SFSP) of a vibration signal measured in multi-directions and multi-positions, the method to extract anomaly signals based on multi-band filter, the symptom parameter optimization method using the least squares mapping (LSM), and the automated successive diagnosis for structural faults of rotating machinery based on multivariate analysis (principal component analysis). In addition, the effectiveness of this approach is discussed and confirmed with experimental data.

Deep learning has great advantages in pattern recognition and has been widely used in many fields, which makes it possible to perform precision diagnosis based on deep learning, especially for precision diagnosis of structure faults. If appropriate signal processing is performed on the diagnostic signal before using deep learning method to diagnosis, the abnormal state recognition accuracy can be further improved. In this study, when the diagnosed raw time domain signal was input to the deep belief neural network (DBN), the accuracy of the diagnosis was low and not sufficient for precise diagnosis. When the frequency domain signal of the raw signal was input to the deep belief neural network, although the accuracy of the diagnosis is greatly improved, the diagnostic accuracy at the low speed is still insufficient to meet the requirements of precision diagnosis. In order to improve the precision of precision diagnosis, we propose a fault information extraction method which combining empirical mode decomposition and sample entropy. When using the method to reconstruct the signal as input, the diagnostic accuracy is extremely good at all speeds, which meet the requirements of precision diagnosis. Based on this method, it is possible to realize the precision diagnosis for structure faults of rotating machinery, and to construct an intelligent diagnostic system for structure faults of rotating machinery. In this study, we will introduce the fault information extraction method based on empirical mode decomposition and sample entropy, the precise diagnosis method based on deep DBN neural network. Then verify the effectiveness of the method by verifying the experiment. Finally, by comparing with the diagnostic results of other diagnostic

techniques, the superiority of the technique relative to other diagnostic methods is discussed and verified.

3. Dynamic analysis of misalignment state

In order to clarify the vibration feature of shaft misalignment, in this paper, in this section, we establish dynamic model of horizontal vibration for angular misalignment state and offset misalignment state, and give the analysis method of exciting forces caused by these states.

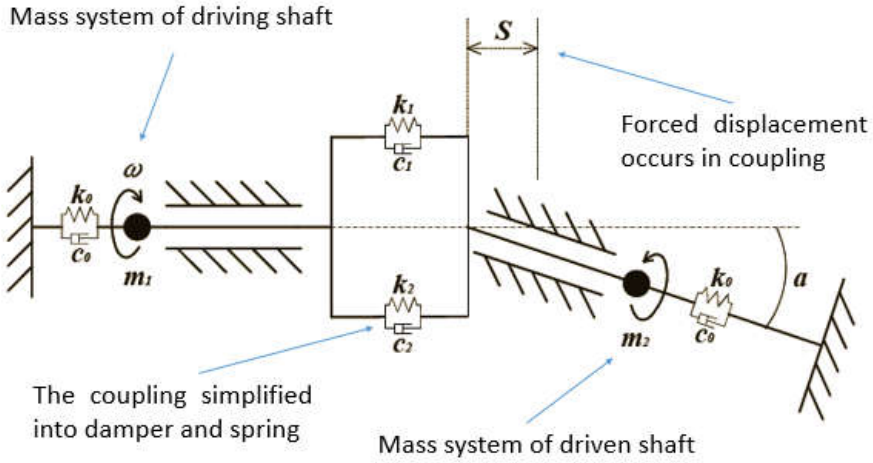

Fig. 2 Angle misalignment

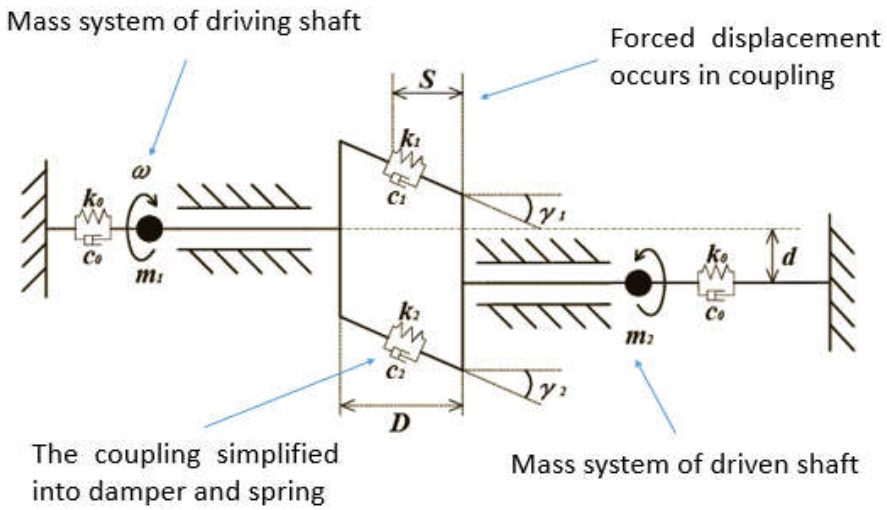

Fig. 3 Offset misalignment

3.1 Dynamic models for misalignment state

3.1.1 Angle misalignment state

To establish the dynamic mode of angle misalignment state, the driving shaft and

driven shaft can be approximately regarded as two mass points (m1 and m2), and connected with spring-damper that fixed two sides as shown in Fig. 4. The bolts of shaft coupling are also replaced by springs and dampers, and the dynamic model has two freedom degrees with spring- damper-mass system. The nonlinear vibration equations of angle misalignment with tow-degree freedom are established as formula (1) and (2).

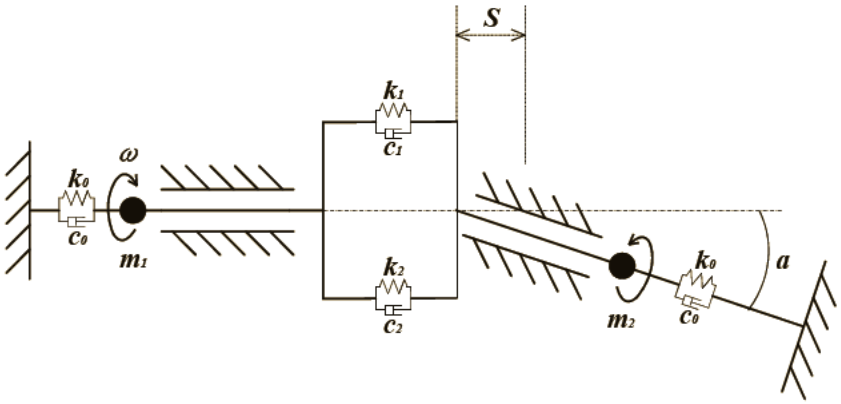

Fig. 4 The dynamic model of angle misalignment state

$$m_1\frac{d^2x}{dt^2}+c_0\frac{dx}{dt}+k_0x+k_1(\mathrm{x}-S_1-x_m\cos\alpha)+k_2(\mathrm{x}-S_2-x_m\cos\alpha)$$
$$+c_1\frac{d(\mathrm{x}-S_1-x_m\cos\alpha)}{dt}+c_2\frac{d(\mathrm{x}-S_2-x_m\cos\alpha)}{dt}=0 \tag{1}$$

$$m_2\frac{d^2x_m}{dt^2}+c_0\frac{dx_m}{dt}+k_0x_m+k_1\cos\alpha(x_m\cos\alpha+S_1-\mathrm{x})+k_2\cos\alpha(x_m\cos\alpha+S_2-\mathrm{x})$$
$$+c_1\frac{d(x_m\cos\alpha+S_1-\mathrm{x})}{dt}\cos\alpha+c_2\frac{d(x_m\cos\alpha+S_2-\mathrm{x})}{dt}\cos\alpha=0 \tag{2}$$

Here, m_1 and m_2 are the masses of the tow shaft, k_0, k_1, and k_2 are spring constants, c_0, c_1, and c_2 are damping coefficients, x and x_m are respectively displacements of the driving shaft and driven shaft, α is the misalignment angle between the driving shaft and driven shaft. S_1 and S_2 are respectively displacements at the springs (k_1, and k_2) and dampers (c_1, and c_2) of the shaft coupling. The exciting forces causing the vibration of the angle misalignment state are caused by S_1 and S_2 while the rotation of the shafts. The derivation method of S_1 and S_2 will be showed in the next chapter.

These vibration equations are used to analyze axial vibration of the angle

misalignment state. The Runge-Kutta method is used to obtain the numerical solution of the equations.

3.1.2 Offset misalignment state

Similarly, the dynamic model of offset misalignment state is also established like angle misalignment state as shown in Fig. 5. The bolts with an inclination angle of γ caused by offset misalignment in the coupling are replaced by springs and dampers. The inclination angle γ in the coupling will produce the exciting force causing vibration while rotating. The nonlinear vibration equations of offset misalignment with tow-degree freedom are established as formula (3) and (4).

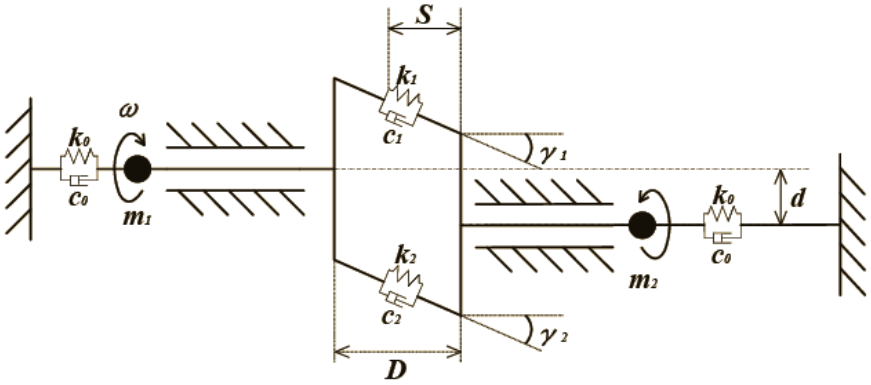

Fig. 5 The dynamic model of offset misalignment state

$$m_1\frac{d^2x}{dt^2}+c_0\frac{dx}{dt}+k_0x+k_1(\mathrm{x}-S_1-x_m\cos\alpha)+k_2(\mathrm{x}-S_2-x_m\cos\alpha)$$
$$+c_1\frac{d(\mathrm{x}-S_1-x_m\cos\alpha)}{dt}+c_2\frac{d(\mathrm{x}-S_2-x_m\cos\alpha)}{dt}=0 \tag{3}$$

$$m_2\frac{d^2x_m}{dt^2}+c_0\frac{dx_m}{dt}+k_0x_m+k_1\cos\alpha(x_m\cos\alpha+S_1-\mathrm{x})+k_2\cos\alpha(x_m\cos\alpha+S_2-\mathrm{x})$$
$$+c_1\frac{d(x_m\cos\alpha+S_1-\mathrm{x})}{dt}\cos\alpha+c_2\frac{d(x_m\cos\alpha+S_2-\mathrm{x})}{dt}\cos\alpha=0 \tag{4}$$

Here, d is the offset distance between two centers of the shafts. γ is the inclination angle between bolts of coupling and driving shaft. S_1 and S_2 are respectively displacements at the springs (k_1, and k_2) and dampers (c_1, and c_2) in the shaft coupling. The exciting forces causing the vibration of the angle misalignment state are caused by S_1 and S_2 (According to the figure above, the forced displacement S of the coupling

contains displacement S_1 and displacement S_2 of each location of coupling) while the rotation of the shafts. The derivation method of S_1 and S_2 will be showed in the next chapter.

These vibration equations are used to analyze axial vibration of the offset misalignment state. The Runge-Kutta method is used to obtain the numerical solution of the equations.

3.2 Displacement analysis of coupling in misalignment state

3.2.1 Displacement analysis of coupling in angle misalignment state

In the case of angle misalignment state, the expansion and the contraction of bolts in the coupling caused by the displacement S shown in Fig. 2 are always changing with initial installed position in the coupling. Fig. 6 shows the initial installed position of the bolts. The number of bolts in this paper is four. In order to calculate the displacement S forcing vibration in the angle misalignment state, we consider the displacement Z_P of the bolt at point P in the direction Z_1 as shown in Fig. 7. The derivation method for the displacement S is shown in the equations (5) to (11).

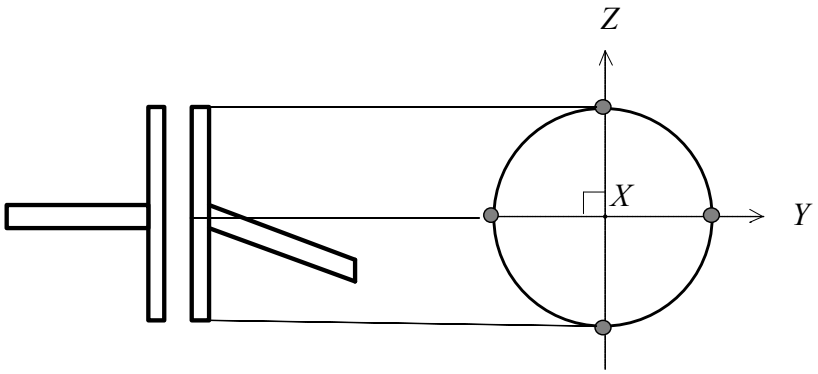

Fig. 6 Initial state of bolt position

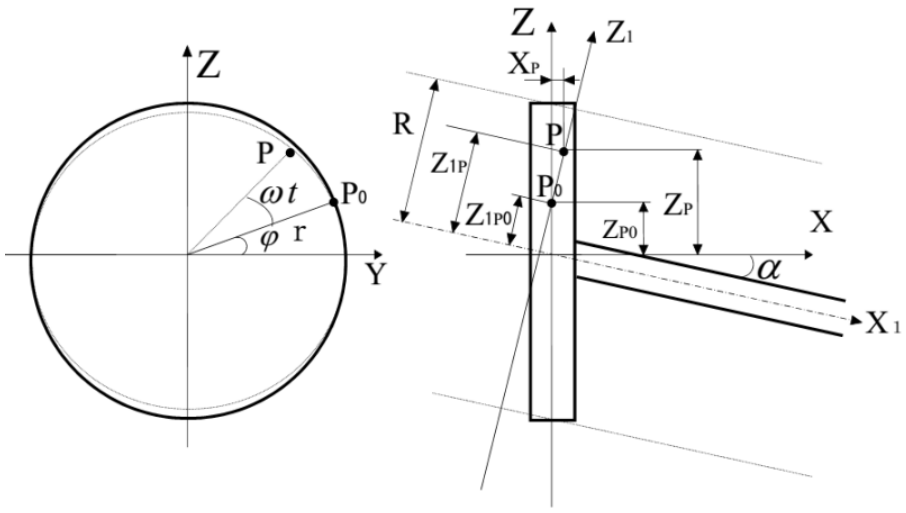

Fig. 7 Displacement of forced vibration of angle misalignment

$$R = r\cos\alpha \tag{5}$$

$$Z_{P0} = r\sin\varphi \tag{6}$$

$$Z_{1P0} = Z_{P0}\cos\alpha = r\sin\varphi\cos\alpha \tag{7}$$

$$Z_{1P} = r\sin(\omega t+\varphi) \tag{8}$$

$$\begin{aligned} Z_P &= Z_{P0} + (Z_{1P} - Z_{1P0})\cos\alpha \\ &= r\sin\varphi + \{r\sin(\omega t+\varphi) - r\sin\varphi\cos\alpha\}\cos\alpha \end{aligned} \tag{9}$$

The displacement S of bolt is:

$$\begin{aligned} S = X_p &= (Z_{1P} - Z_{1P0})\cos\alpha \\ &= r\{\sin(\omega t+\varphi) - \sin\varphi\cos\alpha\}\sin\alpha \end{aligned} \tag{10}$$

The differentiation dS of S is:

$$\frac{dS}{dt} = r\omega\sin\alpha\cos(\omega t+\varphi) \tag{11}$$

S and dS are necessary for the dynamic analysis of the misalignment state.

3.2.2 Displacement analysis of coupling in offset misalignment state

In the case of offset misalignment state, the displacements S in bolts do not change with the installed positions in the coupling. The bolts are replaced by springs as shown in Fig. 8.

Setting the center of coupling A on driving shaft as the coordinate origin, the center of the coupling B on driven shaft, and the coordinates of point P and Q can be

calculated by the following formula.

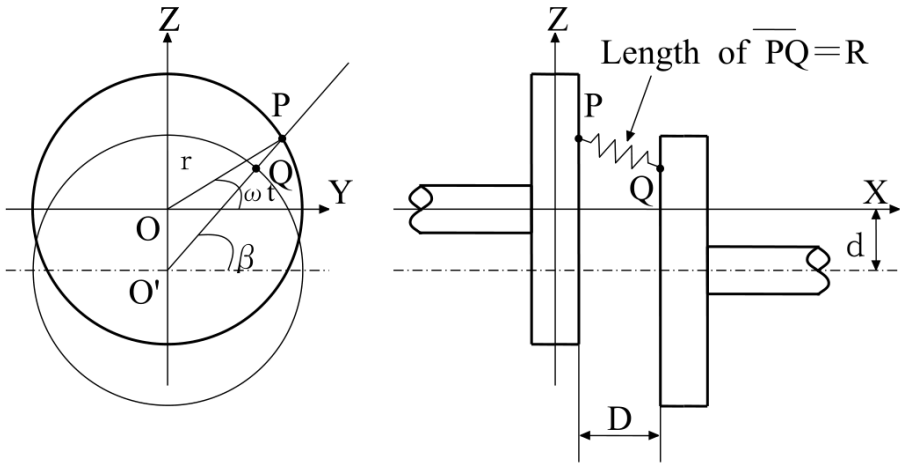

Fig. 8 Displacement of forced vibration of offset misalignment state

$$P = \begin{Bmatrix} P_x \\ P_y \\ P_z \end{Bmatrix} = \begin{Bmatrix} 0 \\ r\cos\omega t \\ r\sin\omega t \end{Bmatrix}, \qquad Q = \begin{Bmatrix} Q_x \\ Q_y \\ Q_z \end{Bmatrix} = \begin{Bmatrix} D \\ r\cos\beta \\ r\sin\beta - d \end{Bmatrix} \tag{12}$$

The distance R between points P and Q is as follows:

$$\begin{aligned} R &= \sqrt{(P_x - Q_x)^2 + (P_y - Q_y)^2 + (P_z - Q_z)^2} \\ &= \sqrt{r^2(\cos\omega t - \cos\beta)^2 + D^2 + (r\sin\omega t - r\sin\beta + d)^2} \end{aligned} \tag{13}$$

Angle β satisfy the following conditions:

$$\tan\beta = \tan\left(\frac{r\sin\omega t + d}{r\cos\omega t}\right) \tag{14}$$

When $\cos\omega t > 0$:

$$\beta = \tan^{-1}\left(\frac{r\sin\omega t + d}{r\cos\omega t}\right) \tag{15}$$

When $\cos\omega t < 0$:

$$\beta = \tan^{-1}\left(\frac{r\sin\omega t + d}{r\cos\omega t}\right) + \pi \tag{16}$$

When $\sin\omega t = 1$:

$$\beta = \frac{\pi}{2} \tag{17}$$

When $\sin \omega t = -1$:

$$\beta = -\frac{\pi}{2} \tag{18}$$

When $\omega t = 0$:

$$\beta_0 = \tan^{-1}\left(\frac{d}{r}\right) \tag{19}$$

The distance R_0 between points P and Q is as follows:

$$R_0 = \sqrt{r^2\left(1 - \frac{r}{\sqrt{r^2 + d^2}}\right)^2 + D^2 + \left(d - r\frac{d}{\sqrt{r^2 + d^2}}\right)^2} \tag{20}$$

The displacement $S_{\overline{PQ}}$ in bolt is:

$$S_{PQ} = R - R_0 \tag{21}$$

The cosine of displacement S in axis direction is:

$$S = \frac{S_{PQ}}{R} D \tag{22}$$

Angle γ between bolt and X-axis is:

$$\gamma = \cos^{-1}\left(\frac{D}{R}\right) \tag{23}$$

Here, S is equivalent to S_1 and S_2 in formula (3) and (4).

3.3 Simulation results and experiment results

The numerical analysis of computer simulation for misalignment state is performed by the dynamic model discussed above and the Runge-Kutta method. When carrying out the computer simulation, the spring constant k of bolts is needed to be decided, and its value is changing with tension or compression while shaft rotating. That is to say, as shown in Fig. 9, when the bolt position in the coupling is in tension state and the bolt is pulled, the spring constant equal to the natural spring constant of the bolt. When bolt position in the coupling is in compression state, because the bolt cannot be compressed due to the bolt hole, the spring constant is equal to the spring

constant of the rubber installed in the coupling. In this paper, the change of the spring constant with coupling rotation is introduced to the dynamic models, so that the characteristics of the misalignment state for the computer simulation are more accurately reflected.

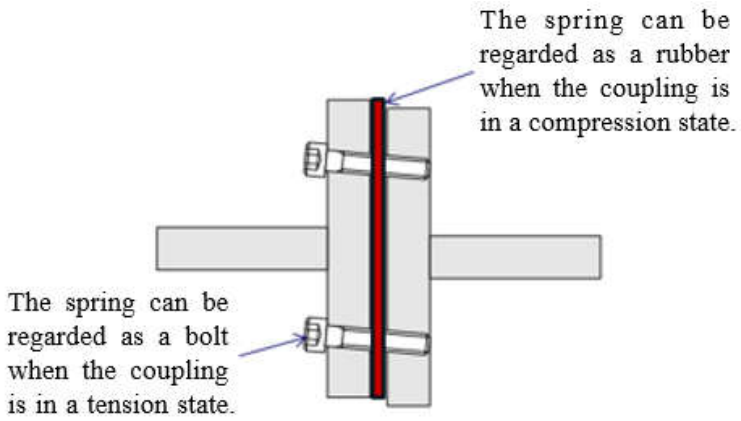

Fig. 9 The spring constant in the bolts

The experiment for verification is carried out to use the rotating machine which consists of rotating shaft, coupling, belt drive, motor and other components, and misalignment states can be set into angle and off-set misalignment as shown in Fig. 10 and Fig. 11. Acceleration signals were measured in normal state and misalignment states by accelerometers. From Fig. 12 to Fig. 47 show the spectrum of the vibration waveform of the angle misalignment state and offset misalignment acquired by simulations respectively.

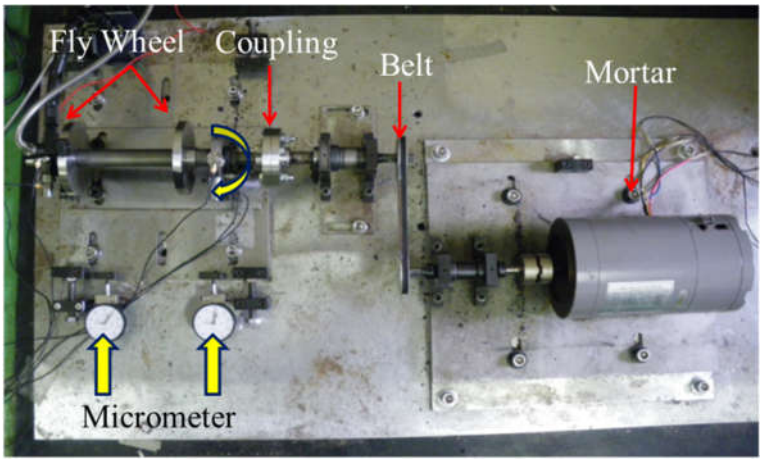

Fig.10 Rotating simulator

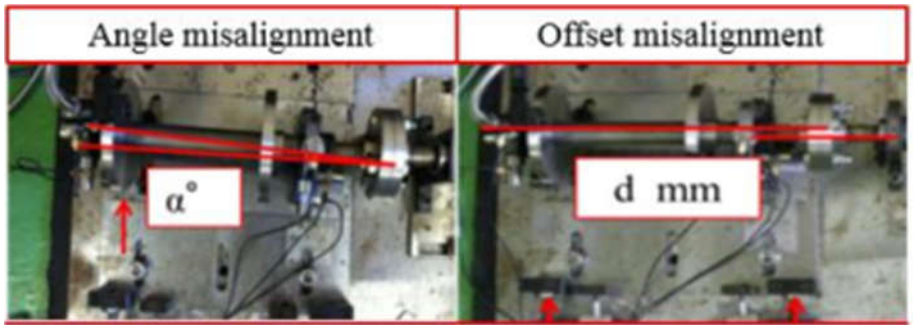

Fig.11 The setting of misalignment states

3.3.1 Simulation results

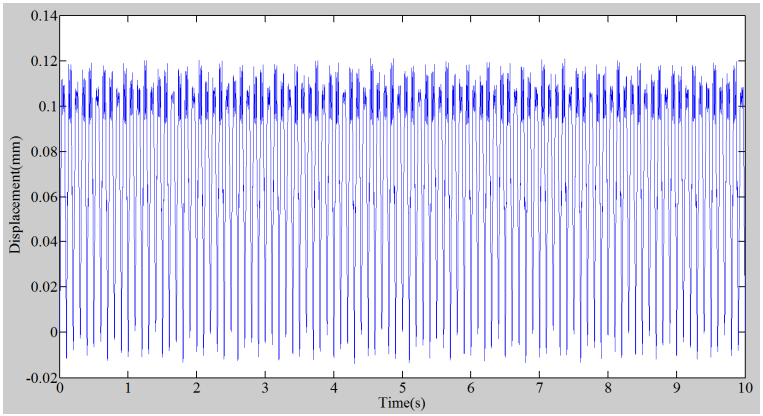

Fig. 12 Raw signal of angle misalignment state for displacement

(Simulation result, a=0.79°, 600rpm)

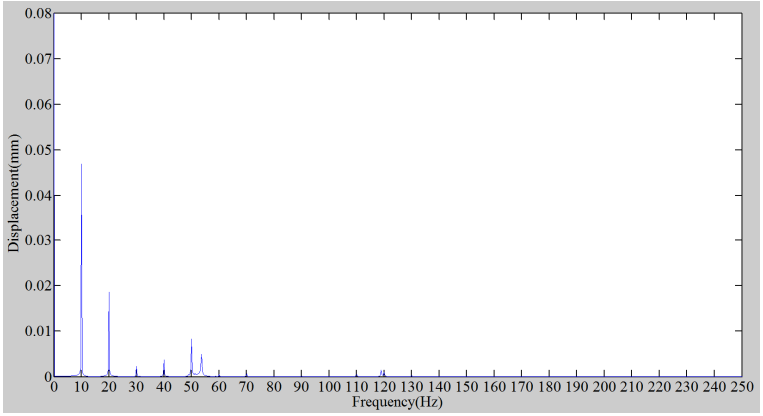

Fig. 13 Spectrum of angle misalignment state for displacement

(Simulation result, a=0.79°, 600rpm)

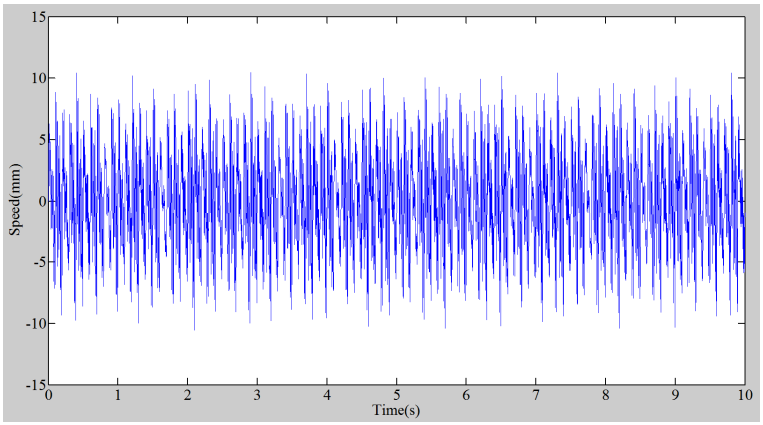

Fig. 14 Raw signal of angle misalignment state for speed

(Simulation result, a=0.79°, 600rpm)

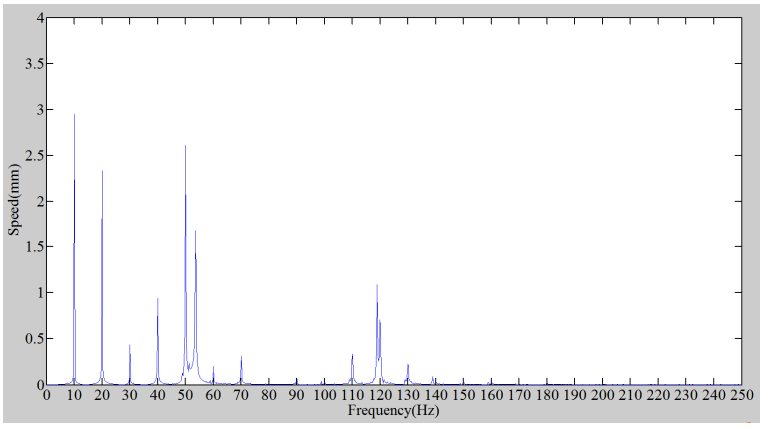

Fig. 15 Spectrum of angle misalignment state for speed

(Simulation result, a=0.79°, 600rpm)

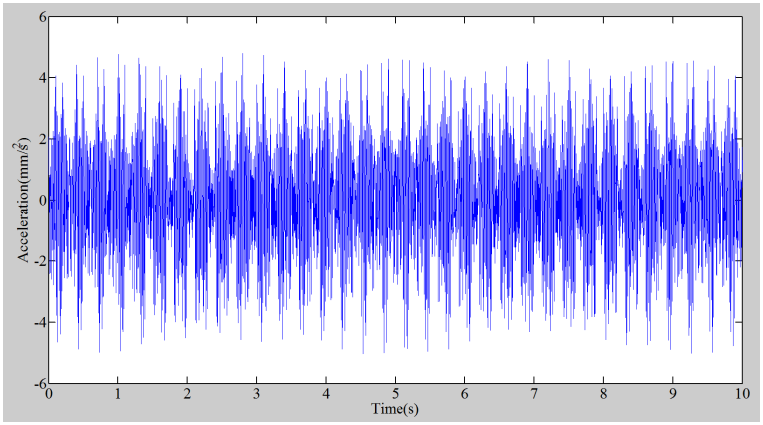

Fig. 16 Raw signal of angle misalignment state for acceleration

(Simulation result, a=0.79°, 600rpm)

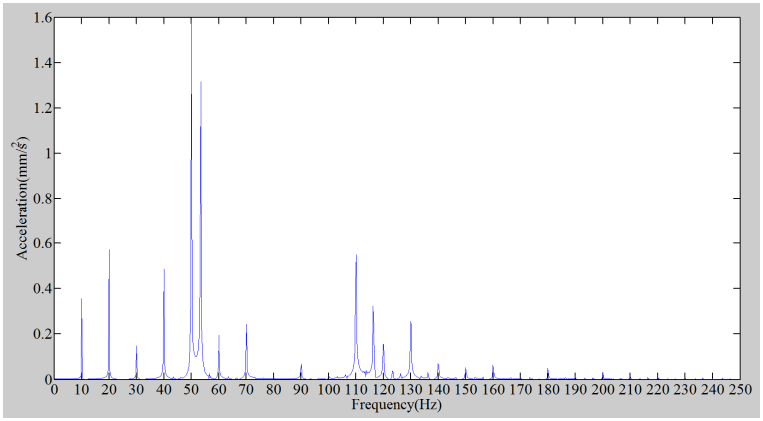

Fig. 17 Spectrum of angle misalignment state for acceleration

(Simulation result, a=0.79°, 600rpm)

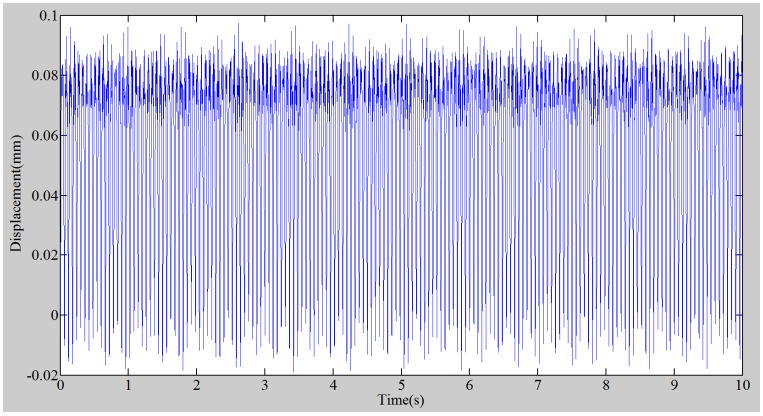

Fig. 18 Raw signal of angle misalignment state for displacement

(Simulation result, a=0.6°, 1000rpm)

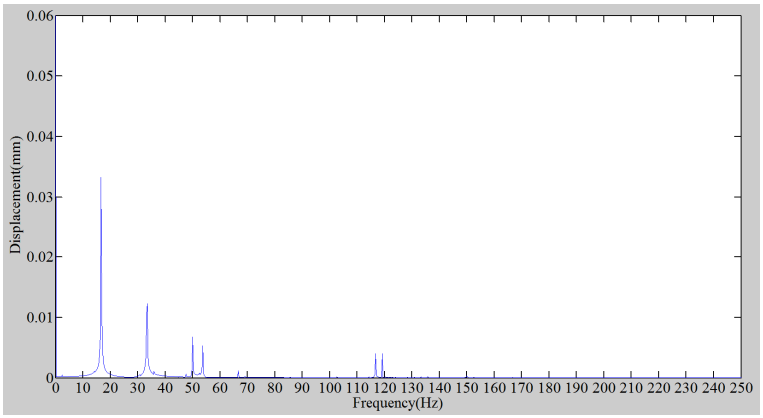

Fig. 19 Spectrum of angle misalignment state for displacement

(Simulation result, a=0.6°, 1000rpm)

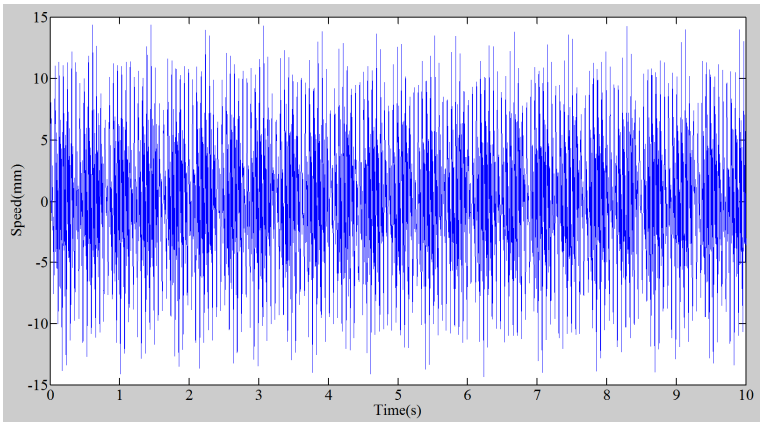

Fig. 20 Raw signal of angle misalignment state for speed

(Simulation result, a=0.6°, 1000rpm)

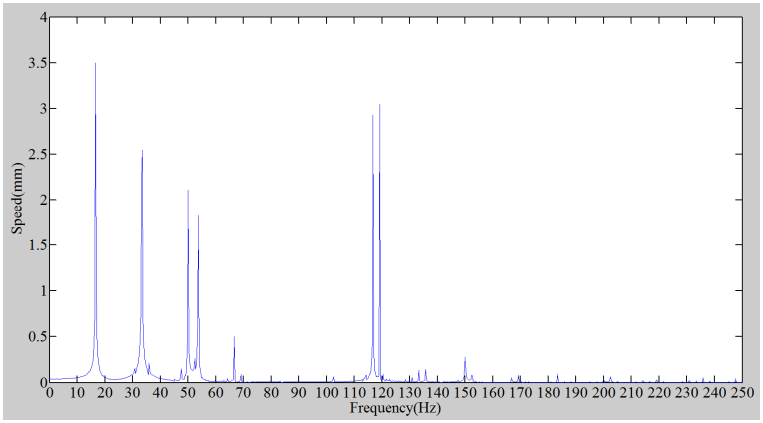

Fig. 21 Spectrum of angle misalignment state for speed

(Simulation result, a=0.6°, 1000rpm)

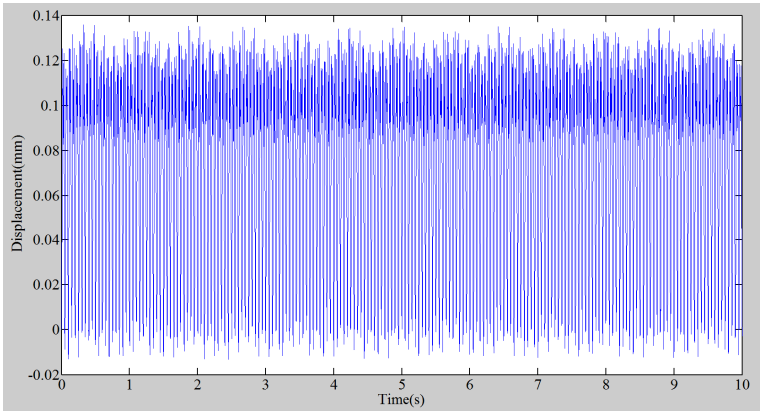

Fig. 22 Raw signal of angle misalignment state for displacement

(Simulation result, a=0.79°, 1200rpm)

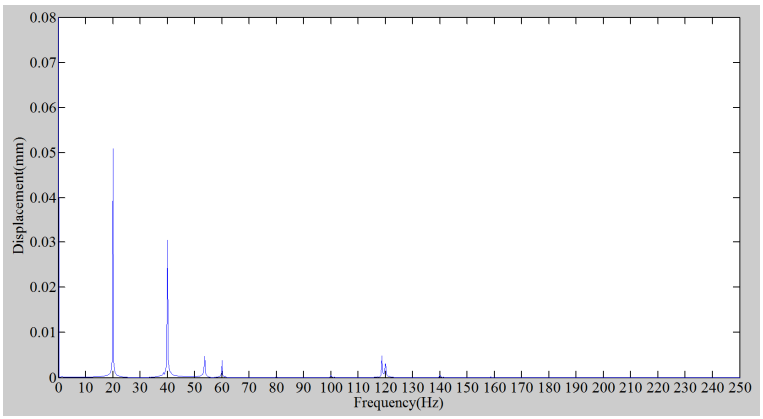

Fig. 23 Spectrum of angle misalignment state for displacement

(Simulation result, a=0.79°, 1200rpm)

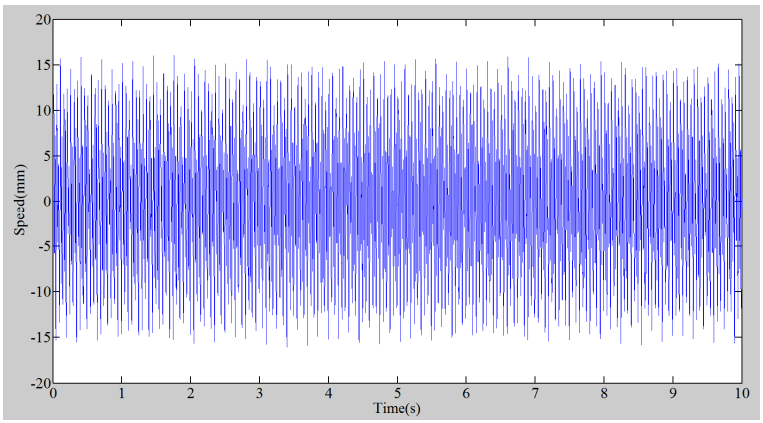

Fig. 24 Raw signal of angle misalignment state for speed

(Simulation result, a=0.79°, 1200rpm)

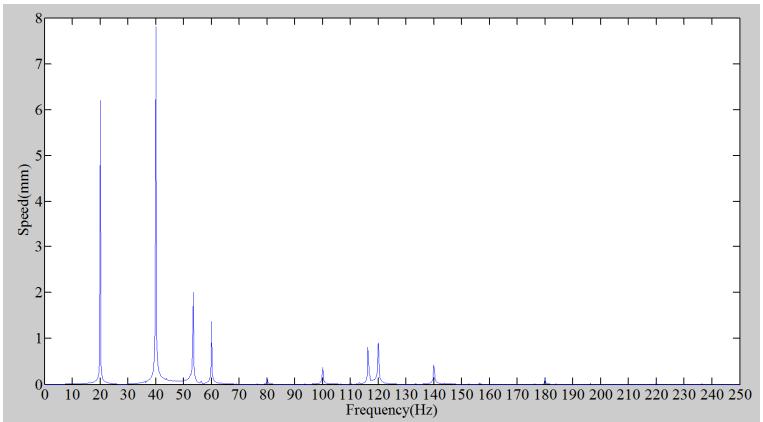

Fig. 25 Spectrum of angle misalignment state for speed

(Simulation result, a=0.79°, 1200rpm)

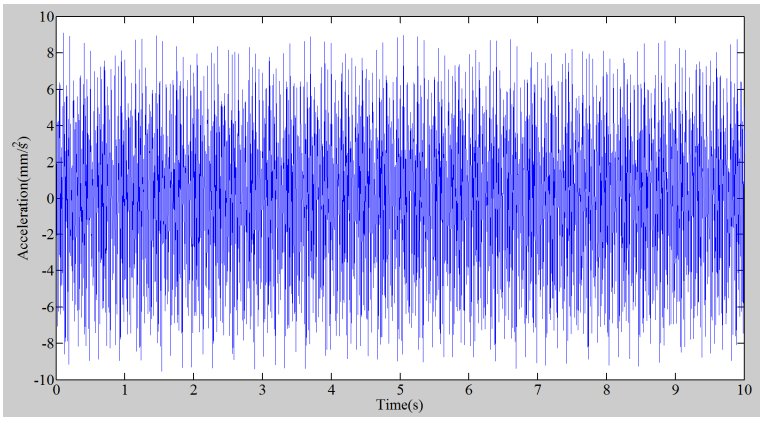

Fig. 26 Raw signal of angle misalignment state for acceleration

(Simulation result, a=0.79°, 1200rpm)

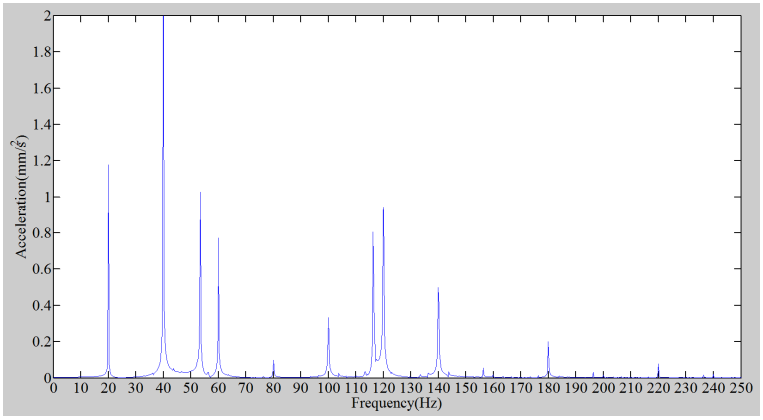

Fig. 27 Spectrum of angle misalignment state for acceleration

(Simulation result, a=0.79°, 1200rpm)

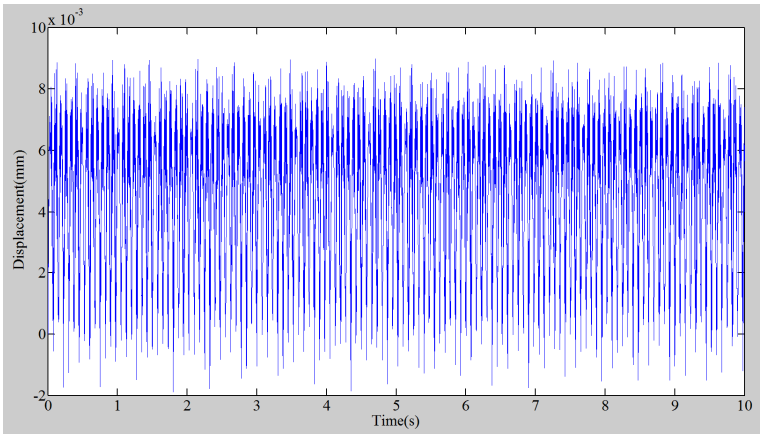

Fig. 28 Raw signal of offset misalignment state for displacement

(Simulation result, d=0.42mm, 800rpm)

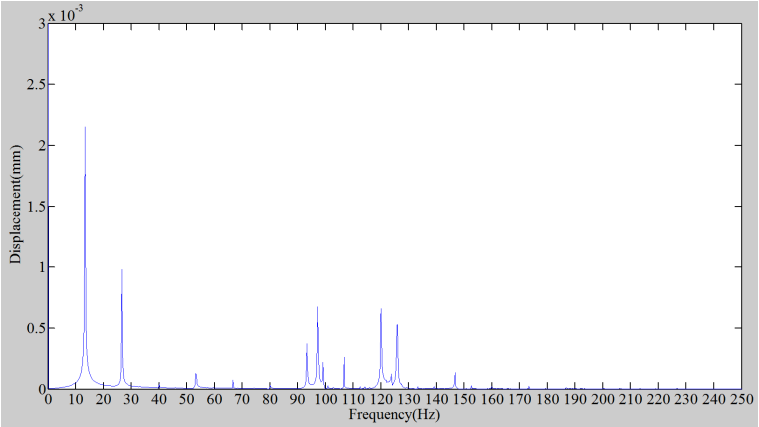

Fig. 29 Spectrum of offset misalignment state for displacement

(Simulation result, d=0.42, 800rpm)

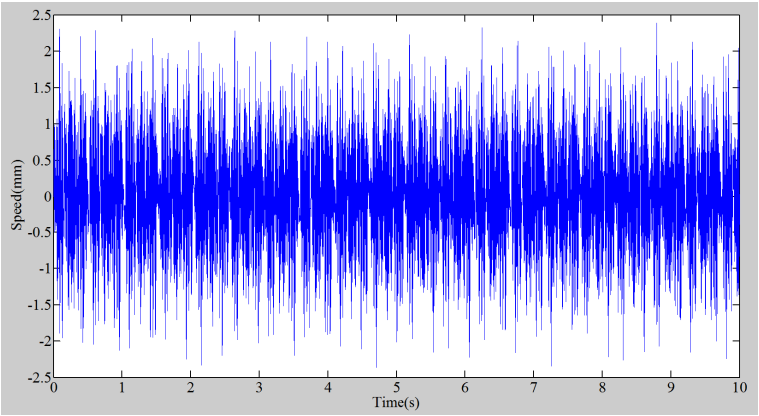

Fig. 30 Raw signal of offset misalignment state for speed

(Simulation result, d=0.42mm, 800rpm)

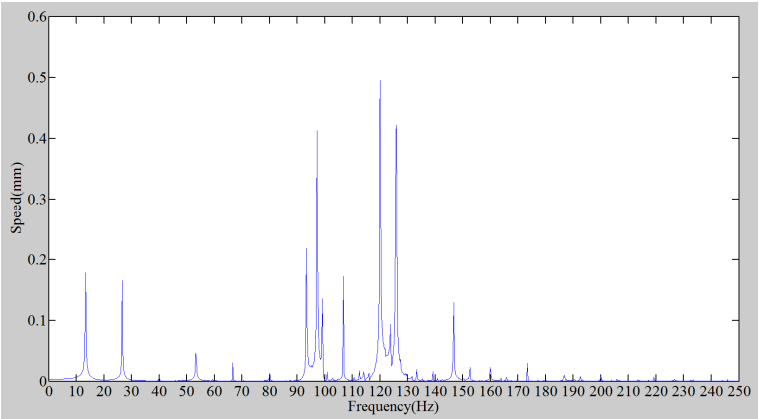

Fig. 31 Spectrum of offset misalignment state for speed

(Simulation result, a=0.42mm, 800rpm)

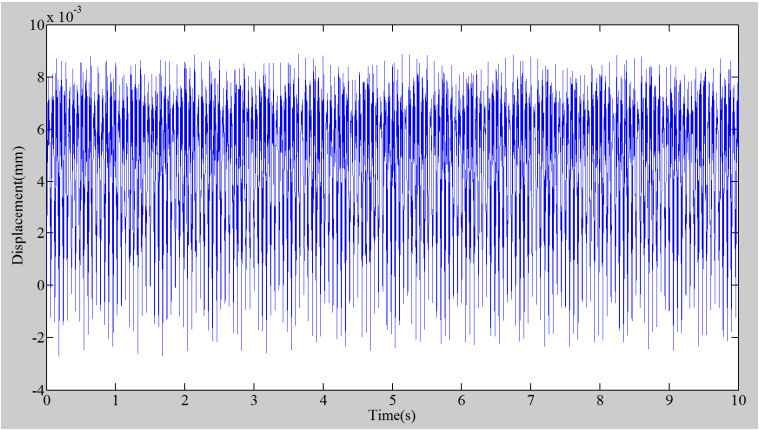

Fig. 32 Raw signal of offset misalignment state for displacement

(Simulation result, d=0.42mm, 1000rpm)

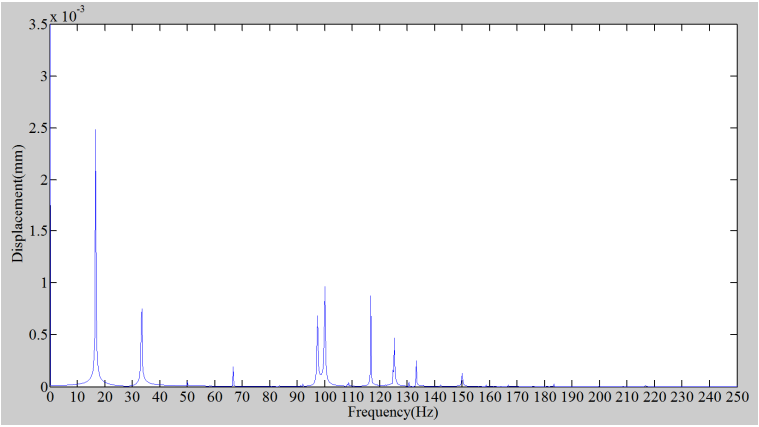

Fig. 33 Spectrum of offset misalignment state for displacement

(Simulation result, d=0.42, 1000rpm)

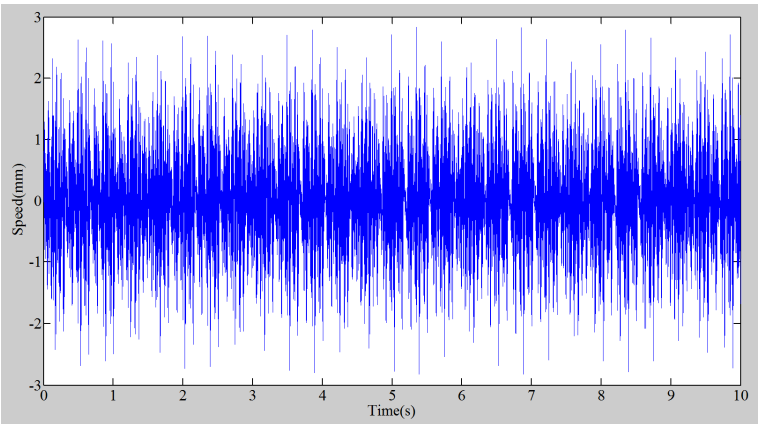

Fig. 34 Raw signal of offset misalignment state for speed

(Simulation result, d=0.42mm, 1000rpm)

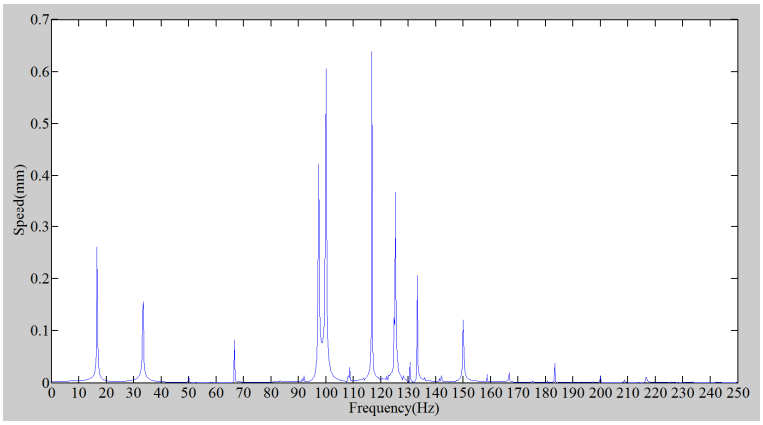

Fig. 35 Spectrum of offset misalignment state for speed

(Simulation result, a=0.42mm, 1000rpm)

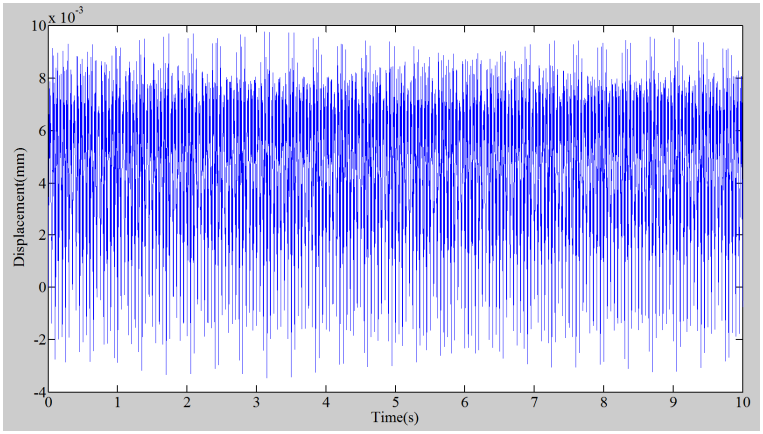

Fig. 36 Raw signal of offset misalignment state for displacement

(Simulation result, d=0.42mm, 1200rpm)

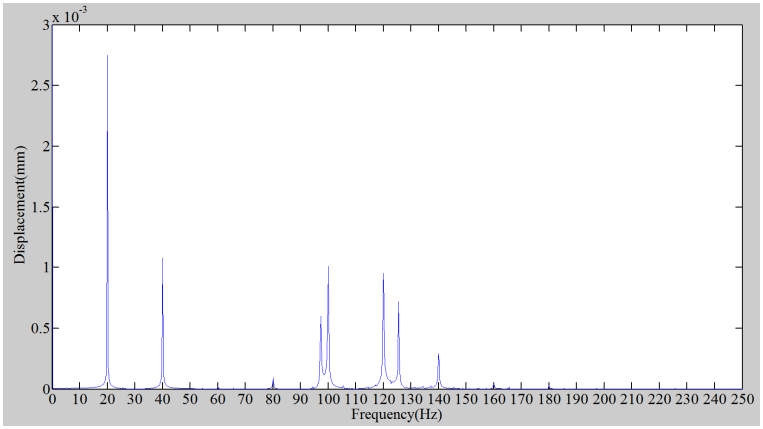

Fig. 37 Spectrum of offset misalignment state for displacement

(Simulation result, d=0.42, 1200rpm)

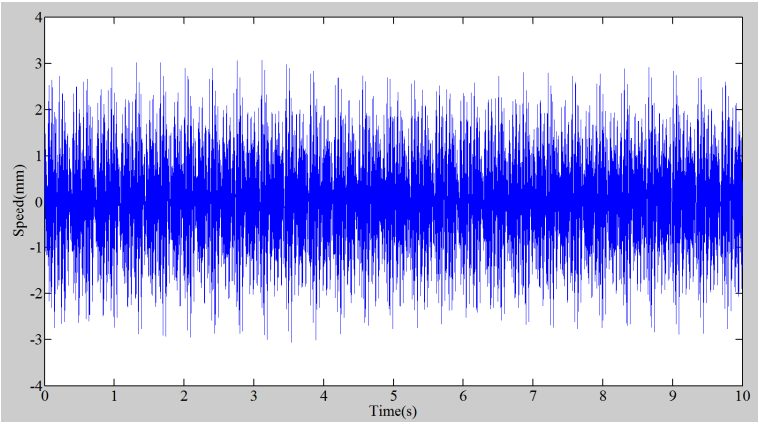

Fig. 38 Raw signal of offset misalignment state for speed

(Simulation result, d=0.42mm, 1200rpm)

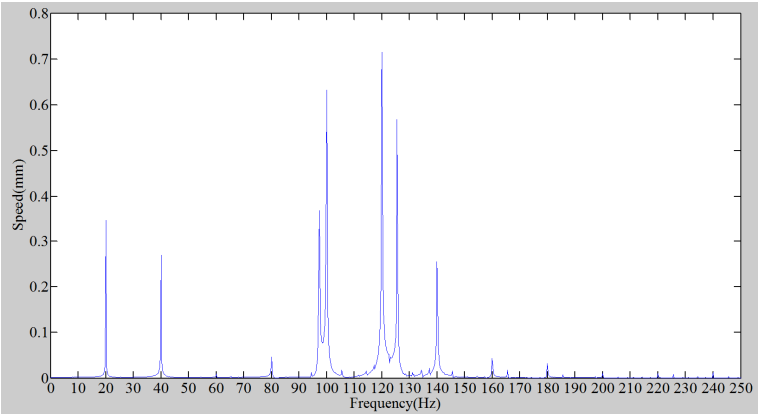

Fig. 39 Spectrum of offset misalignment state for speed

(Simulation result, a=0.42mm, 1200rpm)

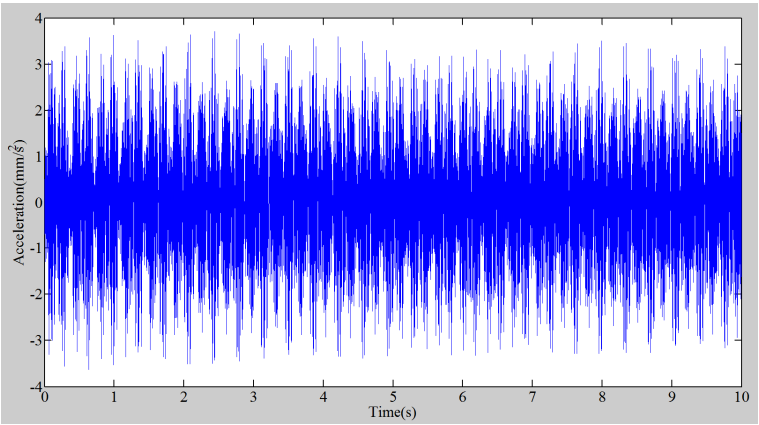

Fig. 40 Raw signal of angle misalignment state for acceleration

(Simulation result, d=0.42mm, 1200rpm)

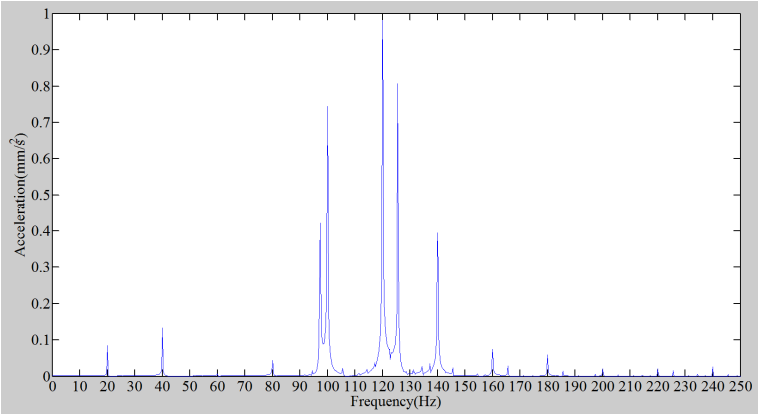

Fig. 41 Spectrum of angle misalignment state for acceleration

(Simulation result, d=0.42mm, 1200rpm)

3.3.2 Experiment results

Since collecting the vibration signal by the acceleration sensor, here, we only show the spectrum of the acceleration signal.

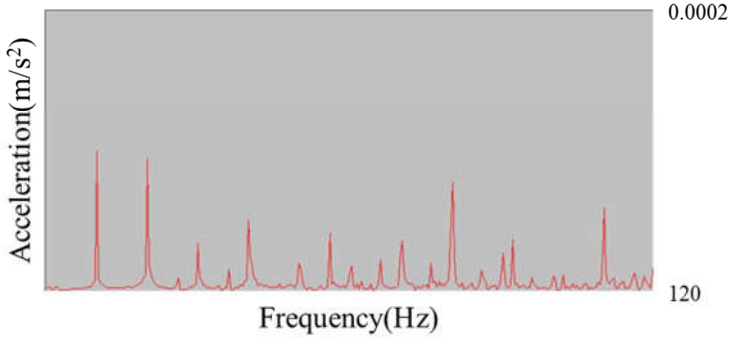

Fig. 42 Spectrum of angle misalignment state for acceleration

(Experiment result, a=0.79°, 600rpm)

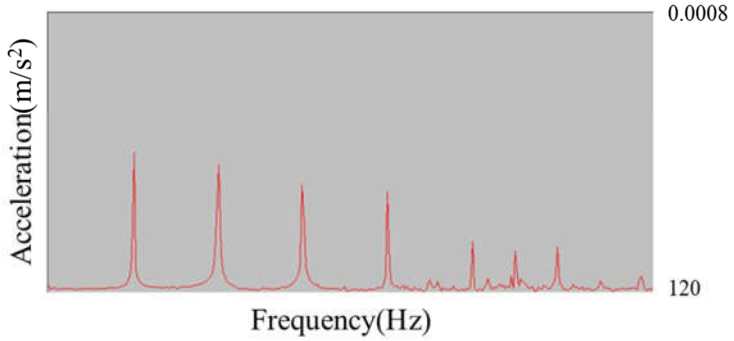

Fig. 43 Spectrum of angle misalignment state for acceleration

(Experiment result, a=0.6°, 1000rpm)

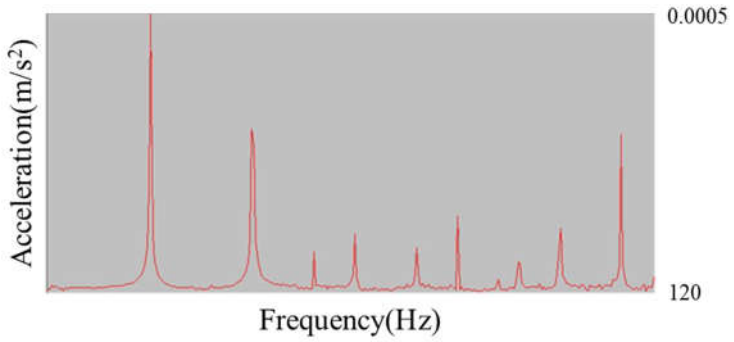

Fig. 44 Spectrum of angle misalignment state for acceleration

(Experiment result, a=0.79°, 1200rpm)

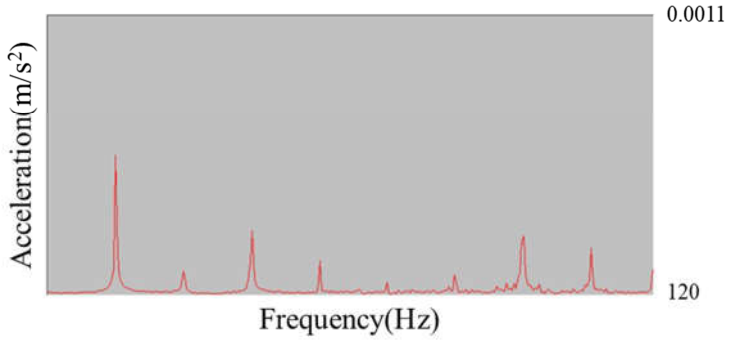

Fig. 45 Spectrum of offset misalignment state for acceleration

(Experiment result, d=0.42mm, 800rpm)

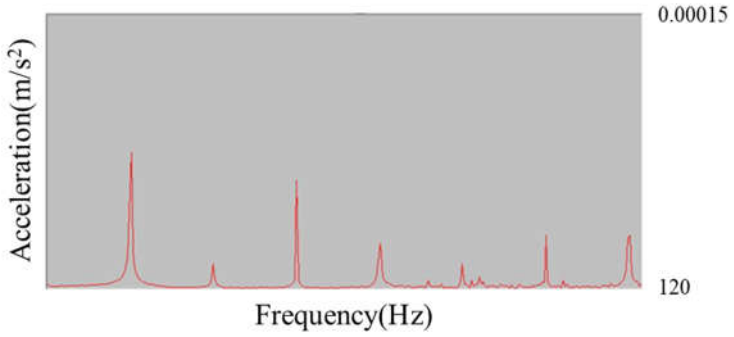

Fig. 46 Spectrum of offset misalignment state for acceleration

(Experiment result, d=0.42mm, 1000rpm)

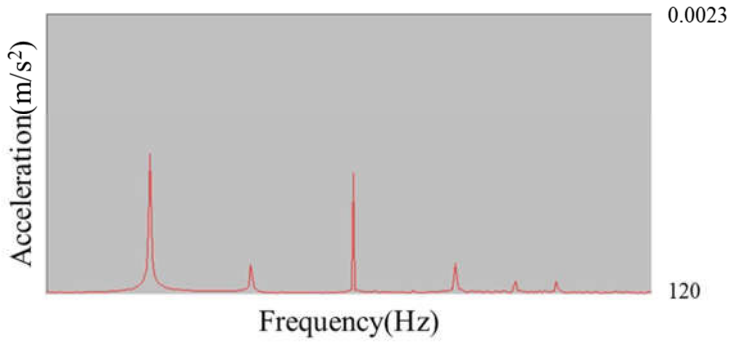

Fig. 47 Spectrum of offset misalignment state for acceleration

(Experiment result, d=0.42mm, 1200rpm)

3.3.3 Comparison of simulation and experiment

From Fig. 12 to Fig. 41 show the raw signal and spectrum of the angle misalignment state and offset misalignment for displacement, speed and acceleration acquired by simulations respectively. From Fig. 42 to Fig. 47 show the spectrum of the angle misalignment state and offset misalignment for acceleration acquired by experiments respectively.

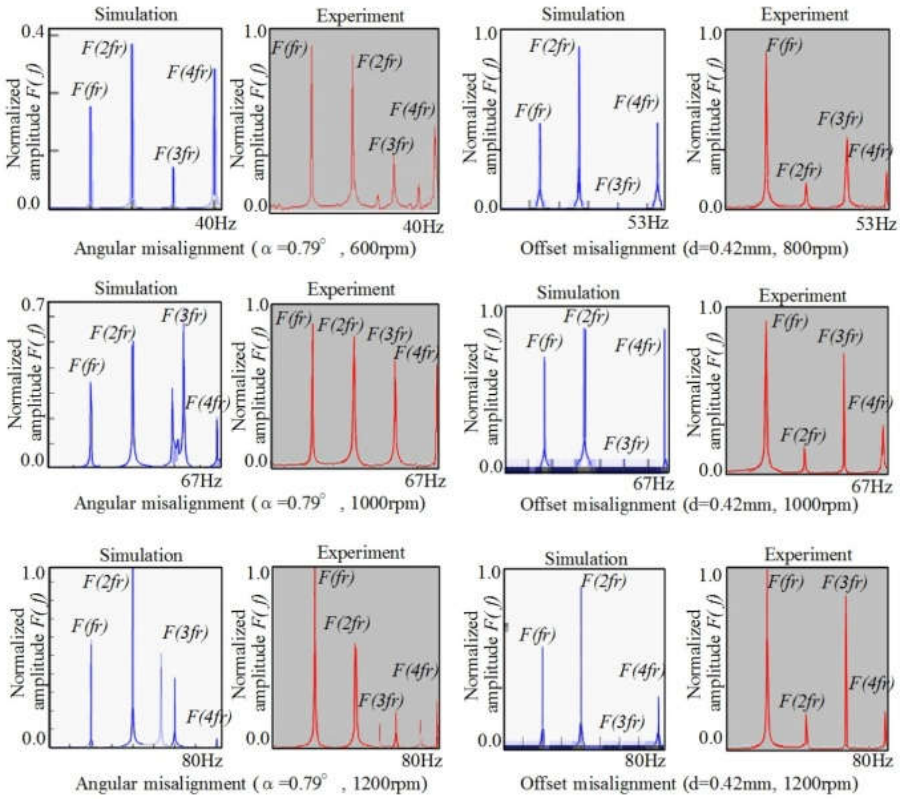

Fig. 48 Spectrum of angle misalignment state for acceleration

(Simulation result, a=0.05°, 1200rpm)

In Fig. 48, the magnitude of spectrum is normalized by the following formula.

$$F(f) = \frac{F'(f)}{\max\limits_{f=0 to 4 f_r} \{F(f)\}} \tag{24}$$

Here, *fr* is rotating frequency, and *F'(f)* is original spectrum calculated from time data by simulation and experiment. Structure fault diagnosis of rotating machinery focuses on the shape of the spectrum but not the magnitude value. For this reason in this study the spectrum is normalized by the formula (24).

Upon misalignment of rotating shaft, with rotation of the shaft, periodic abnormal vibration will be generated, with its characteristic in the frequency spectrum normally occurring in the low frequency zone: apparent peaks are seen at frequency of *N/60* (N is shaft rotation speed) and its multiples. This is an important characteristic that can be used to differentiate normal state and misalignment state. Also, based on different abnormity states, its frequency spectrum has different characteristics.

From these results shown in Fig. 48, in the case of misalignment state, the spectrum $F(f_r)$ at the rotation frequency f_r and its harmonic components $F(2f_r)$, $F(3f_r)$ *and* $F(4f_r)$ are often appear both the results of simulations and experiments. The feature that the peaks in the spectrum appeared at the rotation frequency and its harmonic components can be used to distinguish normal state and other structure faults for rotating machinery. This verifies effectiveness of this dynamic vibration model. However, due to the difficulty of identifying the coefficients of springs (k_1, and k_2) and dampers (c_1, and c_2) in real machine precisely, the amplitudes at the rotation frequency and the harmonic frequencies obtained by the experiments are not perfectly matched with the results of simulations. Based on characteristics of this frequency spectrum, normal state and shaft misalignment state can be readily differentiated, and effectiveness of this dynamic vibration model can be verified. Also, this proves that the spring coefficient and the damping coefficient only affect amplitude of the characteristic frequency spectrum, not its position (frequency in Hz); that is to say, precision diagnosis of rotating shaft structural faults is not significantly affected.

3.4 Method of distinguishing structure faults of rotating machinery

Unbalance, misalignment and looseness are called “structural faults” which often occur in rotating machinery with a feature spectrum in the low frequency area. Structural faults cause shafts to bear excessive fatigue and are the main reason of subsequent failures in other parts, such as bearings and gears. That is to say, structural faults can cause the machinery system to break down and may lead to serious human and economic losses. Therefore, detecting and distinguishing structural faults are extremely important for guaranteeing production efficiency and plant safety. However, because the features of structural faults resemble each other in the vibration signal spectrum in many cases, they are difficult to distinguish. Therefore, we proposed the distinguishing method for structural faults using symptom parameters (SPs) in time domain and spectra of vibration signals according to the simulation and experimental results. (Based on frequency spectrum features demonstrated by misalignment dynamic vibration model and experiment proposed earlier, we hereby propose a diagnosis method combining time domain characteristic parameters with frequency spectral analysis for diagnosis of rotating shaft structural faults).

The states to be diagnosed for the rotating simulator are normal, misalignment, unbalance and looseness. The misalignment state can be set by adjusting the shafts. The unbalance state can be set by placing an unbalanced hammer on the flange, and the looseness state by adjusting the tightness of the bolts at the bearing box and pedestal as shown in Fig. 49. The accelerometers shown in Fig. 50 are used to measure vibration signals in the vertical, horizontal and axial directions. The vibration signals are measured at constant speeds (600, 900 and 1200rpm) and the sampling frequency of signal measurement is 5 kHz.

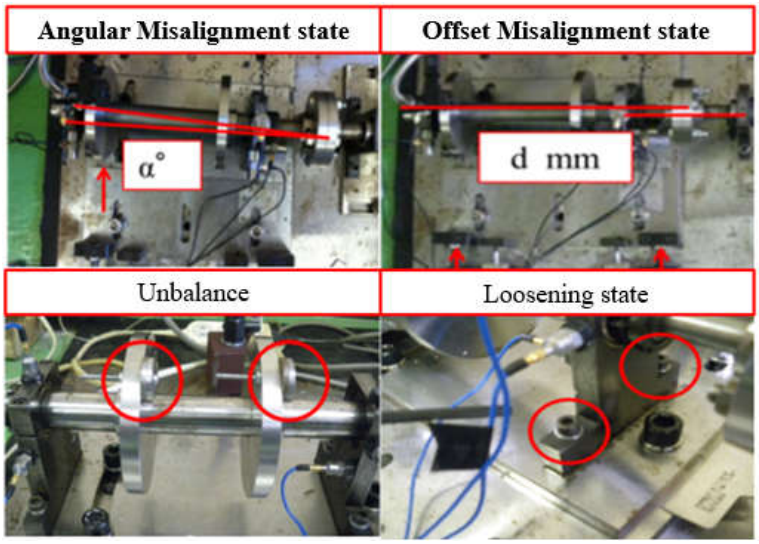

Fig. 49 Adjustment of structural faults

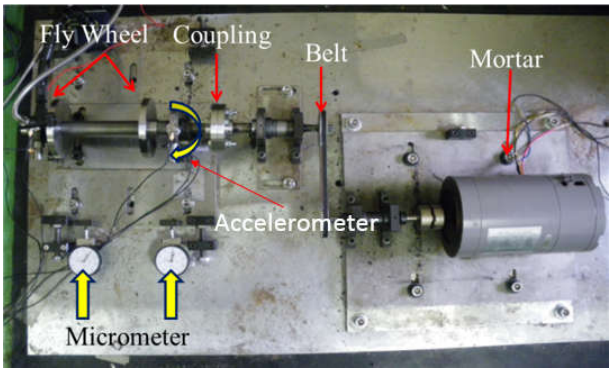

Fig. 50 Rotation simulator and misalignment states

The conclusion for diagnosing the structure faults by results of the simulation and the experiments are as follows:

(1)The vibration features of each state are resemble in the horizontal and axial directions by seeing the spectra shown in Fig. 51 and Fig. 52. Also, this feature further verifies rationality of the model proposed earlier that only involves axial vibration.

(2) The spectra of misalignment and looseness are very resembled, but different from unbalance state.

(3) The method for distinguishing these states is shown henceforth:

i) Unbalance state: the peak value in the spectrum appears at the rotating frequency f_r, and the magnitude will become larger with the rotating speed. Based on this frequency spectral characteristic, unbalance state can be differentiated from the other two states in structural faults.

ii) Misalignment state: the peak values in the spectrum appear at the rotating frequency f_r and its harmonic frequency $i\,f_r$.

iii) Looseness state: the peak values in the spectrum also appear at the rotating frequency f_r and its harmonic frequency $i\,f_r$.

iv) Since the frequency spectrum of misalignment state is very similar to that of the looseness state, these two cannot be directly differentiated according to frequency spectrum. In order to distinguish misalignment state and looseness state; two symptom parameters, standard deviation and skewness shown in following formulas (25) and (26), should be used.

$$\sigma = \sqrt{\sum_{i=1}^{N}\left(x_i - \bar{x}\right)^2 \Big/ N} \tag{25}$$

$$\beta = \sum_{i=1}^{N}\left(x_i - \bar{x}\right)^3 \Big/ N \tag{26}$$

Here, x_i is the data digital data of the vibration signal, and N is the number of the signal. This diagnosis method uses axial vibration signals to calculate aforesaid characteristic parameters.

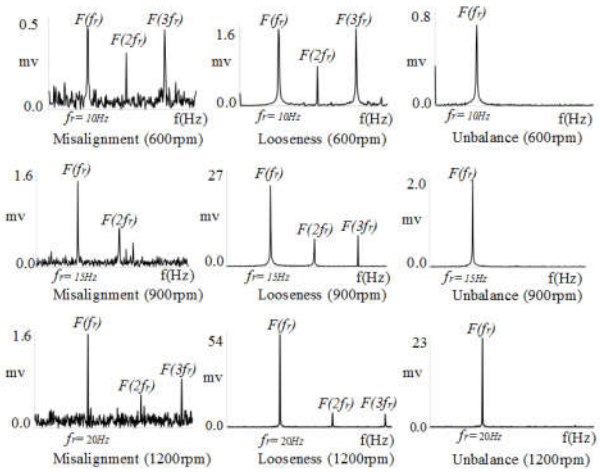

Fig. 51 Spectrum of abnormal states in horizontal direction

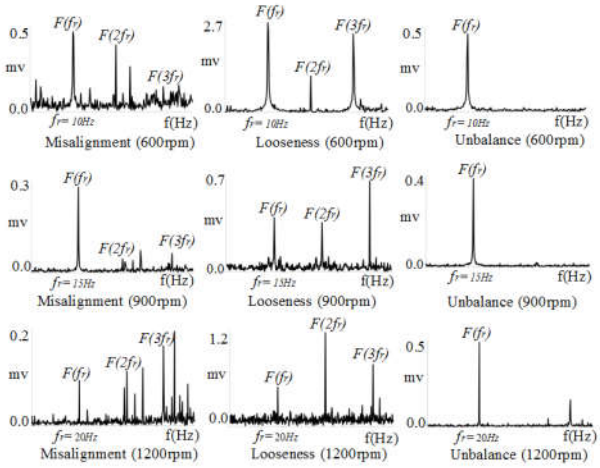

Fig. 52 Spectrum of abnormal states in axial direction

The values of the two symptom parameters calculated from the vibration signal measured in each state are shown in Fig. 53 and Fig. 54. By these figures, the values of the standard deviation and the skewness of looseness state are larger than that of other states. They become larger and larger with increases in the rotation speed. The reason can be explained that when the looseness state occurs, shocking vibration also occurs at the loosened bolt, and the shape of the vibration signal became asymmetric as shown in Fig. 55. To sum up, the unbalance state can be diagnosed by the spectrum, and the misalignment state and looseness state can be distinguished by the spectrum and the symptom parameters (σ and β). Further, this makes identification of three types of structural faults possible.

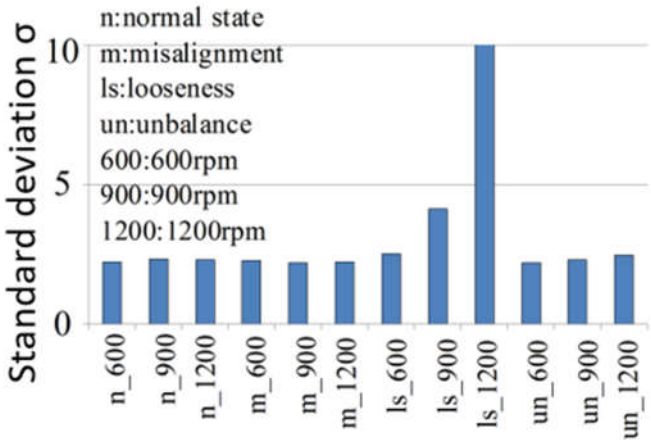

Fig. 53 Standard deviation of different states and speeds

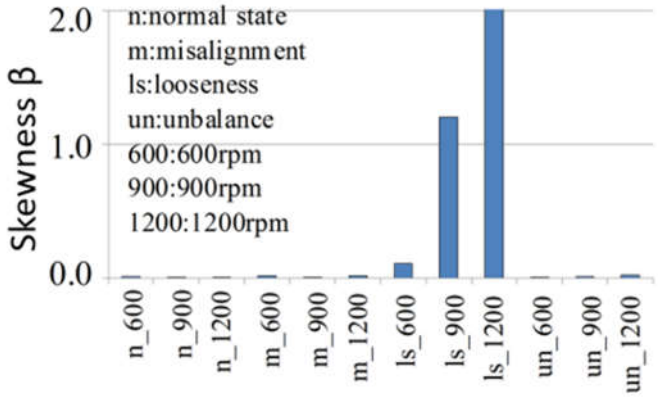

Fig. 54 Skewness of different states and speeds

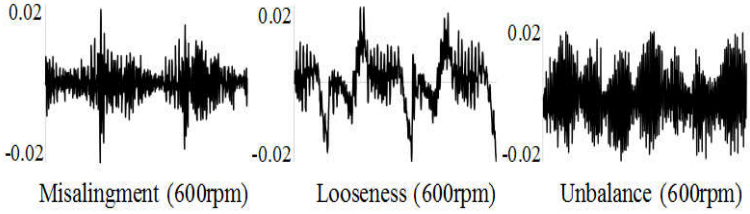

Fig. 55 Time signals of abnormal states

3.5 Summary

In this research, the dynamic models of axial vibration of shaft misalignment state were proposed. In order to obtain the solution of the dynamic models and clarify the feature of the vibration signal in misalignment states, the method for calculating the vibration displacement caused by each misalignment state was showed. The computer simulation and experiment using rotating machine were also shown to verify the efficiency of the dynamic analysis method proposed in this paper. The features of the vibration signal of misalignment states can be clarified and the mechanism of occurrence of misalignment states can be explained theoretically based on the dynamic models.

Finally, the method for distinguishing structure faults of rotating machinery (shaft misalignment state, unbalance state and looseness state) was discussed by using symptom parameters and spectrum of the vibration signal measured in these states. The method is proved to be effective to distinguish structure faults of rotating machinery.

We will continue studying the dynamic analysis concerning the looseness state

theoretically, and report the results in subsequent studies (including the diagnosis method that uses new characteristic parameters).

4. Fault diagnosis method for structure faults of rotating machinery by multi-positional and multi-directional signals fusion and sequential successive multivariate analysis

4.1 Diagnostic theory and method

The structural faults of the rotating machine include those caused by such mechanical structural defects as unbalance, misalignment, and loosening of the fasteners, resulting in abnormal vibration at a relatively low frequency. As the most common faults in rotating machinery, structural faults not only have direct adverse effects on the performance of the equipment and the quality of the product, but also cause excessive stress on the peripheral components such as bearings and gears [16], leading to secondary faults. This makes it extremely vital to realize that fault detection and type identification of structure faults states are very important to ensure machine safety and production quality [17].

Compared to the normal state, the most common feature of the structural faults is the changes of the spectrum of vibration signal in the rotational frequency and its harmonic components. Although some studies have revealed part of spectral characteristics of a series anomalous state, it is still insufficient to accurately draw a distinguishing line between different structural faults. In view of this, it is often very difficult to determine the anomaly types (precision diagnosis), especially an effective automatic diagnosis method has not yet been established in the diagnostic system. When the intelligent condition diagnostic system is developed via computer algorithms, the symptom parameters are required to express the characteristics of the vibration signal measured to distinguish the states of the machinery. Nonetheless, in the computer-based automatic diagnosis, especially at the early stage of structural faults, the noise of the measured vibration signal is very strong, therefore the anomaly identification sensitivity of symptom parameters commonly used in statistics (kurtosis, skewness, wave height, etc.) has remained low for long time. In other words, it would be difficult to detect the anomalies and distinguish their types by using these commonly used symptom parameters. Furthermore, as the automatic detection method

of the structural faults based on conventional neural network is affected by noise, the data learned are fuzzy. Consequently, the learning by the neural network often cannot ensure the convergence, resulting in many difficulties in building a practical diagnosis system.

Currently dimensional or non-dimensional symptom parameters are widely used for fault diagnosis such as abnormal of centrifugal pump, rolling element bearing and so on. Therefore, to effectively and automatically detect and identify the structural faults that may be present with the rotating machinery, in the present method, the structural feature symptom parameters are calculated from the multi-position & multi-direction vibration signals, which were measured in the normal state (reference state) and the unknown state. The symptom parameters of high sensitivity can be selected by detection index (DI), and then optimized by the least squares mapping method. Through the principal component analysis, these symptom parameters can be integrated, and are used as the basis for anomaly detection and identification of types of anomalies. The flow of the diagnosis is shown in Fig. 56. The output determines all the diagnosed states.

That is to say, as shown in Fig. 56, in the different stages of learning, the normal state is taken as the reference state at first. The vibration signals measured in the unknown state (the state being diagnosed) at multiple directions and multiple positions can be extracted by the multi-band filter to obtain the rotation frequency and the high order harmonic components, followed by the calculation of the symptom parameters. After selecting the symptom parameters of high sensitivity by DI, optimization can be performed by LSM and the principal component analysis is carried out to obtain the first principal component and the second principal component in the unknown state. It is the same to obtain the first principal component and second principal component for identifying each abnormal state when abnormal states are taken as the reference state, as in the case of the processing flow where the normal state is taken as the reference state.

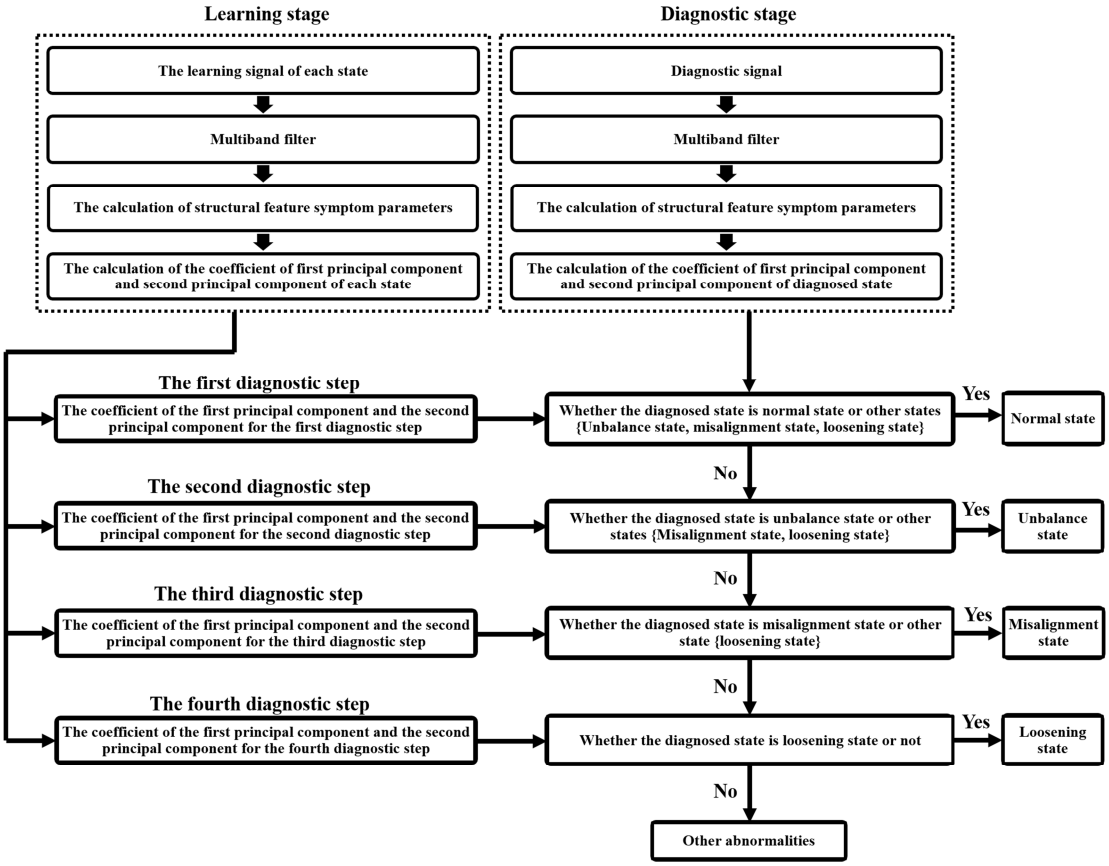

Fig. 56 Automated successive learning - Diagnostic process

At the time of diagnosis, the vibration signal is also obtained from the multi-direction and multi-position measurement, followed by calculation of symptom parameters. This process up to this point is the same as that of the learning stage. The first diagnosis step is to obtain the first principal component and the second principal component with reference to the normal state, to determine whether the diagnosed state is normal state. If yes, the diagnosis ends. For abnormal state, it goes to the second diagnostic step. In the second diagnostic step, the first principal component and the second principal component are obtained with the unbalanced state as the reference, to determine whether this abnormal state is unbalance state or not. If yes, the diagnosis ends. If not, the successive diagnosis will continue from the third step until the abnormal state is identified.

4.2 Structural feature symptom parameters

In this research, to accurately diagnose the structural faults, new symptom parameters called “Structural Feature Symptom Parameter (SFSP)” are defined by the following formulas.

(1) Axial vibration index p_{s1}:

$$p_{s1} = (A_{ad} / A_{rd}) / (A_{an} / A_{rn}) \tag{27}$$

A_{ad}: Axial vibration level at diagnosis;

A_{rd}: Radial vibration level at diagnosis;

A_{an}: Axial vibration level in normal state;

A_{rn}: Radial vibration level in normal state;

(The rotation frequency component, the effective value and the average peak may all be used as the vibration level)

(2) For every 100rpm, the amplitude increase ratio p_{s2}:

$$p_{s2} = \{P_2(f_r) / P_1(f_r)\} / \{(N_2 - N_1) / 100\} \tag{28}$$

N_1, N_2: Rotating speed (rpm), $N_2 - N_1 > 200$ rpm.

$P_1(f_r)$, $P_2(f_r)$: The rotation frequency component respectively at the rotating speed N_1 and N_2, .

(3) Rotation frequency component rate p_{s3}:

$$p_{s3} = \{P_d(f_r) / \sum_{i=2}^{20} P_d(if_r)\} / \{P_n(f_r) / \sum_{i=2}^{20} P_n(if_r)\} \tag{29}$$

$P_d(fr)$, $P_n(fr)$: The rotation frequency component at diagnosis and in normal state, respectively.

$P_d(if_r)$, $P_n(if_r)$: The higher harmonic components of the rotation frequency at diagnosis and in normal state.

(4)2Sub-harmonic rate p_{s4}:

$$p_{s4} = \{P_d(2f_r) / P_d(f_r)\} / \{P_n(2f_r) / P_n(f_r)\} \tag{30}$$

$P_d(fr)$, $P_n(fr)$: The rotation frequency components at diagnosis and in normal state, respectively.

$P_d(2fr)$, $P_n(2fr)$: 2 times of the harmonic component for the rotation frequency respectively at diagnosis and in normal state.

(5) Third Sub-harmonic Rate p_{s5}:

$$p_{s5} = \{P_d(3f_r) / P_d(f_r)\} / \{P_n(3f_r) / P_n(f_r)\} \tag{31}$$

$P_d(fr)$, $P_n(fr)$: The rotation frequency components at diagnosis and in normal state, respectively.

$P_d(3fr)$, $P_n(3fr)$: 3 times of the harmonic component for the rotation frequency respectively, at diagnosis and in normal state.

(6) High-order Sub-harmonic Rate p_{s6}:

$$p_{s6} = \{\sum_{i=4}^{10} P_d(if_r) / P_d(f_r)\} / \{\sum_{i=4}^{10} P_n(if_r) / P_n(f_r)\} \quad (32)$$

$P_d(fr)$, $P_n(fr)$: The rotation frequency components at diagnosis and in normal state, respectively.

$P_d(ifr)$, $P_n(ifr)$: i times of the harmonic component for the rotation frequency respectively at diagnosis and in normal state,.

(7) Vertical and Horizontal Amplitude Ratio p_{s7}:

$$p_{s7} = (A_{vd} / A_{hd}) / (A_{vn} / A_{hn}) \quad (33)$$

A_{vd}, A_{vn}: Vertical vibration level respectively at diagnosis and in normal state;

A_{hd}, A_{hn}: Horizontal vibration level respectively at diagnosis and in normal state;

(8) Vertical Amplitude Ratio on the left and right p_{s8}:

$$p_{s8} = (A_{lvd} / A_{rhd}) / (A_{lvn} / A_{rhn}) \quad (34)$$

A_{lvd}, A_{lvn}: The left vertical vibration level respectively at diagnosis and in normal state;

A_{rhd}, A_{rhn}: The right vertical vibration level respectively at diagnosis and in normal state;

(9) Horizontal amplitude ratio on the left and right p_{s9}:

$$p_{s9} = (A_{vd} / A_{hd}) / (A_{vn} / A_{hn}) \quad (35)$$

A_{vd}, A_{vn}: The left horizontal vibration level respectively, at diagnosis and in normal state;

A_{hd}, A_{hn}: The right horizontal vibration level respectively at diagnosis and in normal state,;

(10) High/low frequency components ratio ps10:

$$p_{s10} = \{\sum_{f>1kH} P_d(f) / \sum_{f\le 1kH} P_d(f)\} / \{\sum_{f>1kH} P_n(f) / \sum_{f\le 1kH} P_n(f)\} \quad (36)$$

$P_d(f)$, $P_n(f)$: The spectrum at diagnosis and in normal state, respectively.

(11) Skewness Difference p_{s11}:

$$p_{s11} = |\beta_d| - |\beta_n| \quad (37)$$

β_d, β_n: The skewness at diagnosis and in normal state, respectively.

(12) Kurtosis difference p_{s12}:

$$p_{s12} = \gamma_d - \gamma_n \quad (38)$$

γ_d, γ_n: The kurtosis at diagnosis and in normal state, respectively.

(13) Noise level p_{s13}:

$$p_{s13} = \{\sum_{i=1}^{6f_r} P_n(f_i) / \sum_{i=1}^{6} P_n(if_r)\} / \{\sum_{i=1}^{6f_r} P_d(f_i) / \sum_{i=1}^{6} P_d(if_r)\} \quad (39)$$

$P_d(f)$, $P_n(f)$: The spectrum at diagnosis and in normal state, respectively.

4.3 Multi-band filter

Since the structural faults will produce relatively low frequency vibration, under which the measured signal in each state will show different frequency components, the filtering process of vibration signal is necessary in order to reduce the influence of noise. In this research, multi-band filtering is performed before the calculation of structural feature symptom parameters as shown in Fig. 56, and the feature signals are extracted. By the so-called multi-band filtering, only the rotating frequency and its high order harmonic components are retained in the spectrum of signals, and the other components are turned to zero. Fig. 59 shows the multi-band filtering with i=5 (retaining the components from the rotating frequency up to the fifth order harmonic frequency of the rotating frequency).

Fig. 57 and Fig. 58 exhibit the original vibration signal and its spectrum. In this research, the components of rotational frequency in the low frequency domain and their high order harmonic components with a region of ±3Hz in width are extracted as the filtered spectrum, as shown in Fig.59, by taking into account the variation of the rotational speed at the time of measuring the vibration signal, then it is converted into a time domain signal. Fig.60 is the filtered time domain signal, and the filtered data are used to calculate the structural feature symptom parameters.

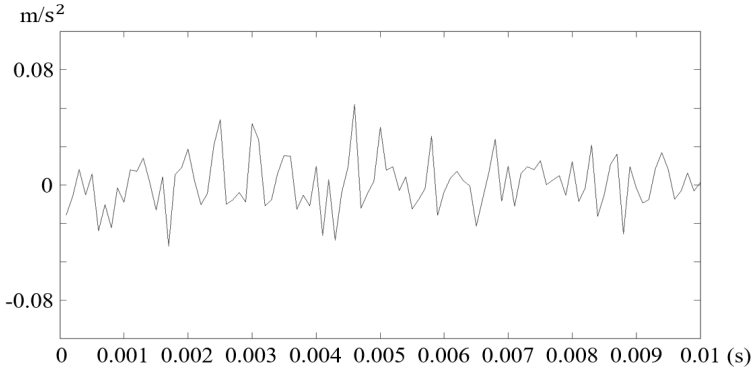

Fig. 57 Original Vibration Signal (normal state)

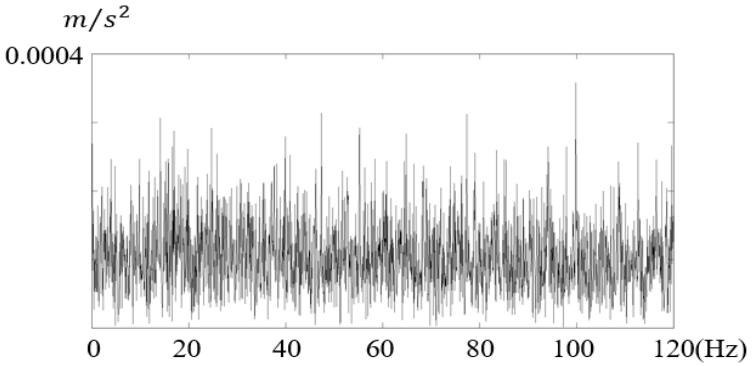

Fig. 58 Spectrum of the Original Vibration Signal

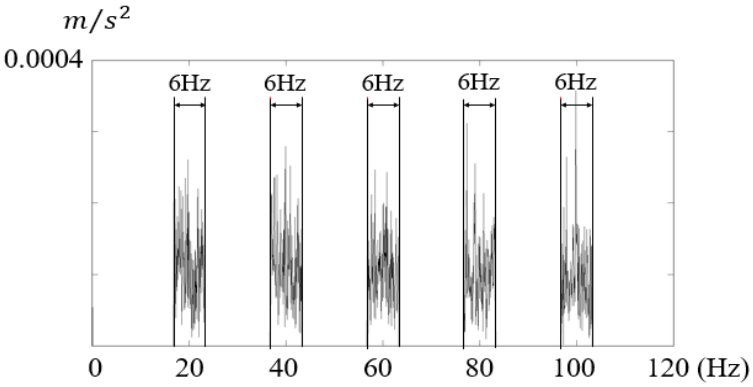

Fig. 59 Multi-band Filtering

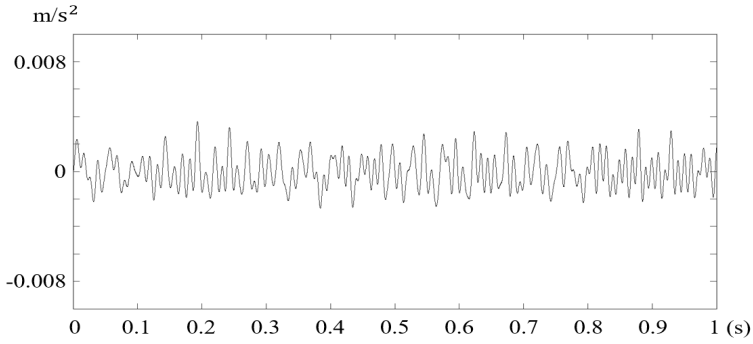

Fig. 60 Filtered Vibration Signal

4.4 Selection and optimization of symptom parameter

To select the structural feature symptom parameters with high diagnosis sensitivity, the *DI* value in the following formula can be used as an identification index to evaluate the diagnosis sensitivity of the symptom parameters.

$$DI = \frac{|\mu_1 - \mu_2|}{\sqrt{\sigma_1^2 + \sigma_2^2}} \tag{40}$$

Here, μ_1 and μ_2 are the averages of symptom parameters *p* (each structural feature symptom parameter *p* has multiple samples) of state 1 (being diagnosed) and state 2 (reference state), and σ_1 and σ_2 indicate the standard deviation of symptom parameters p at state 1 and state 2. The larger *DI* value, the higher diagnosis sensitivity of the symptom parameter in identifying state 1 and state 2.

In this work, the least squares mapping method is also used to enhance the diagnosis sensitivity of structural feature symptom parameters. That is, the high-sensitivity structural feature symptom parameters may be obtained by the univariate linear regression of the least squares mapping method [18]. This methodology is demonstrated by the following formula. n- The number of samples representing the symptom parameters.

i - The sample number of each of the symptom parameters.

y - The size of each sample.

Y - The size of each sample after optimization.

a and b - Respectively represent the slope and intercept of the ideal linear equation.

As an example, structural feature symptom parameters before and after optimization of sensitivities are shown in Fig.61. Being Improved by Using the Least Squares Mapping Method with Those without being improve.

$$b = \bar{y} - a\bar{x} \tag{41}$$

$$Y = ax + b \tag{42}$$

$$a = \frac{\sum_{i=1}^{n} x_i y_i - n\overline{xy}}{\sum_{i=1}^{n} x_i^{\,2} - n\bar{x}^{2}} = \frac{\sum_{i=1}^{n}\left(x_i - \bar{x}\right)\left(y_i - \bar{y}\right)}{\sum_{i=1}^{n}\left(x_i - \bar{x}\right)} \tag{43}$$

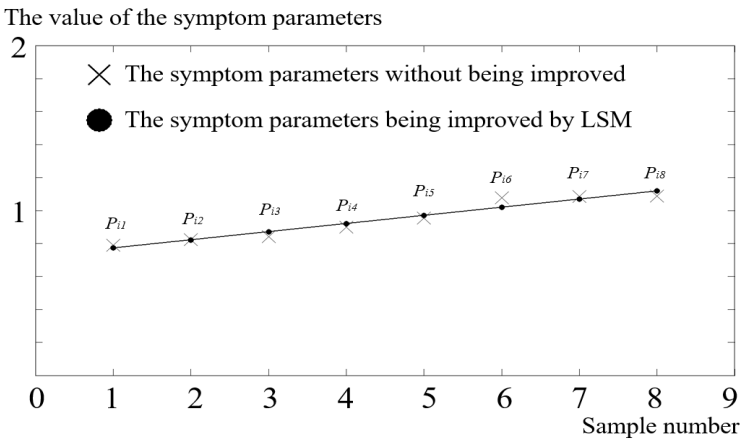

Fig. 61 Comparison of the Symptom Parameters

4.5 Principal component analysis of symptom parameters

Before using the principal component to integrate the structural feature symptom parameters, it is necessary to first standardize the calculated symptom parameters *(ps1'~psm')* in the following way.

$$p_{si} = \frac{p_{si}' - p_{sin}}{Sp_{sin}} \tag{44}$$

Here, p_{sin} and Sp_{sin} present the average value and standard deviation of the structural feature symptom parameters p_{si}' in the normal state (reference state) respectively. The principal components (the size is m) are represented by the following equation.

$$\begin{Bmatrix} z_1 \\ \vdots \\ z_m \end{Bmatrix} = \begin{bmatrix} a_{11} & \cdots & a_{1m} \\ \vdots & \cdots & \vdots \\ a_{n1} & \cdots & a_{nm} \end{bmatrix} \begin{Bmatrix} p_1 \\ \vdots \\ p_m \end{Bmatrix} = AP \tag{45}$$

Here, A is the correlation coefficient matrix, and the coefficients a_{ij} are obtained from the data in the normal state (reference state). Furthermore, the eigenvalues of the covariance matrix obtained from the structural feature symptom parameters p_{si} in the normal state are denoted by λ_1-λ_i, and λ_i is the standard deviation of the i*th* principal component.

4.6 Experimental verification

4.6.1 Setting the experimental equipment and structural faults

Fig. 62 shows the rotating machine simulator that can be used to simulate the structural faults of the rotating machinery, and the laser alignment meter which is used to set the normal state and the misalignment states. As illustrated in Fig. 63, the vibration acceleration signals were measured in five directions (left vertical, right vertical, left horizontal, right horizontal, and axial) on two bearing housings. In the signal measurement, the sampling frequency was 5000Hz, and the rotating speed was respectively 600rpm, 900rpm and 1200rpm.

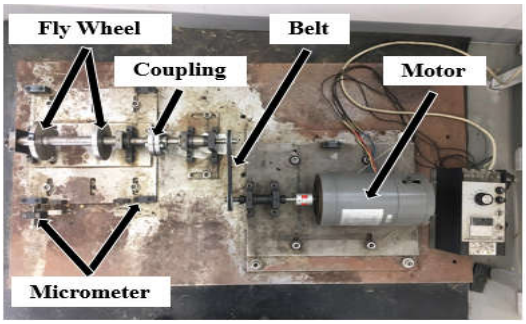

(a) Rotating Machinery Simulator

(b) Laser alignment meter

Fig. 62 The rotating machinery simulator and the laser alignment meter

As illustrated in Fig. 64, the set states of structural faults are misalignment state, unbalance state, and loosening state. The misalignment state can be set by adjusting the position and angle of the rotating shaft. The unbalance state can be set by setting the unbalanced hammer in the flange. The loosening state can be set by adjusting the tightness the bolts of the bearing housing and pedestal.

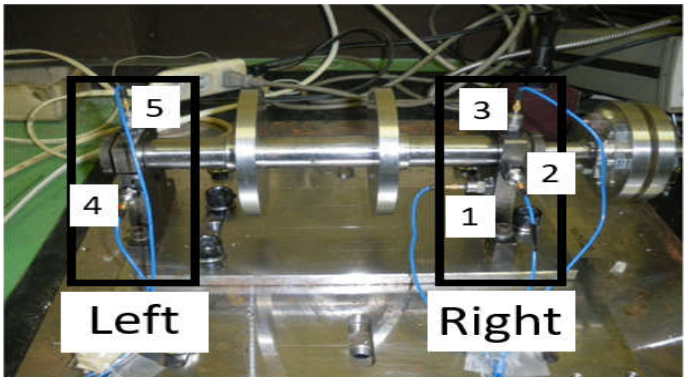

Fig. 63 Measurement of vibration signals in five directions

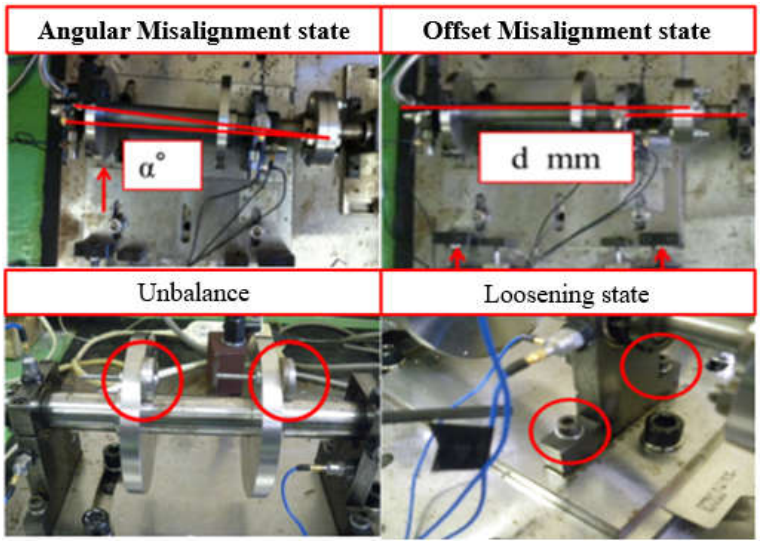

Fig. 64 An Example of setting the structural faults at the rotation simulator

4.6.2 Results of successive diagnosis based on principal component analysis

Fig. 65 ~ Fig. 68 illustrate the results of successive diagnoses based on principal component analysis. Figure 65 shows the diagnosis results with reference to the normal state to determine whether a state is normal or not. The horizontal axis represents the first principal component, and the vertical axis represents the second principal component. Based on the principal component analysis, the structural feature symptom parameters of all diagnosed states were integrated into the first and second principal components, and the results were plotted in the coordinate system. Points close to the origin stand for the states are close to the normal state (or the reference state), and points of other states fall far away from the origin. In Figure 65, the first principal component and the second principal component in the normal state are shown with a confidence interval of 99.9% ($\overline{X} \pm 3\sigma_1, \overline{Y} \pm 3\sigma_2$). In other words, if a point of the diagnosed state falls outside this interval, it can be determined that the state is abnormal with a confidence level of 99.9%. The symbols in the figure are shown below.

N state: Normal state

SU state: Static unbalanced state

DU state: Dynamic unbalanced state

AM state: Angular misalignment state

OM state: Offset misalignment state

CL state: Loosening state

In Fig. 65, points representing abnormal states are located outside this confidence interval ($\overline{X} \pm 3\sigma_1, \overline{Y} \pm 3\sigma_2$), and points of the respective abnormal states are gathered in their own areas.

The same as the normal state described above, Fig. 66, Fig. 67 and Fig. 68 show, respectively, the diagnostic results whether the diagnosis state was the reference state or not when the angular misalignment state, the offset misalignment state, and the loosening state were used as the reference. In particular, for structural faults with slight deviations, such as angular misalignment and offset misalignment, dynamic unbalance

and static unbalance, their points were often found present in adjacent areas in the coordinate system. According to these features, the detection of structural faults and anomaly type identification based on multivariate analysis and successive diagnosis can be realized.

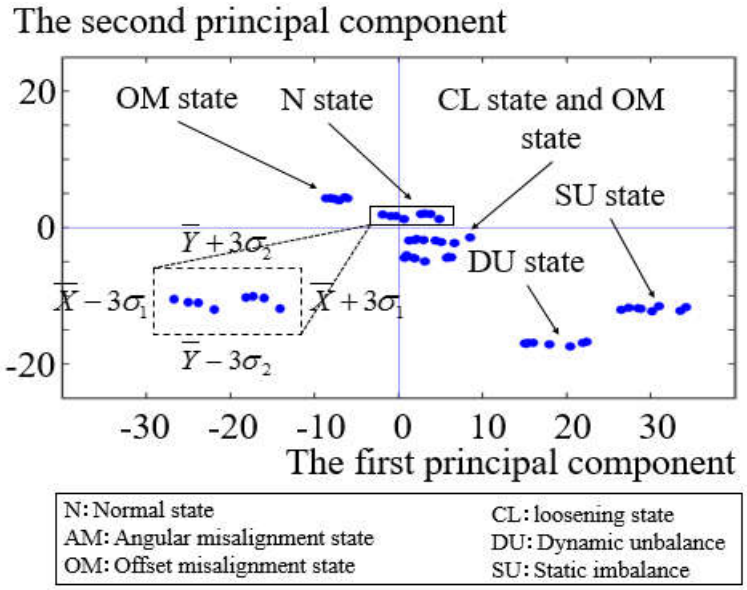

Fig. 65 Results of the Principal Component Analysis with the Normal State as Reference

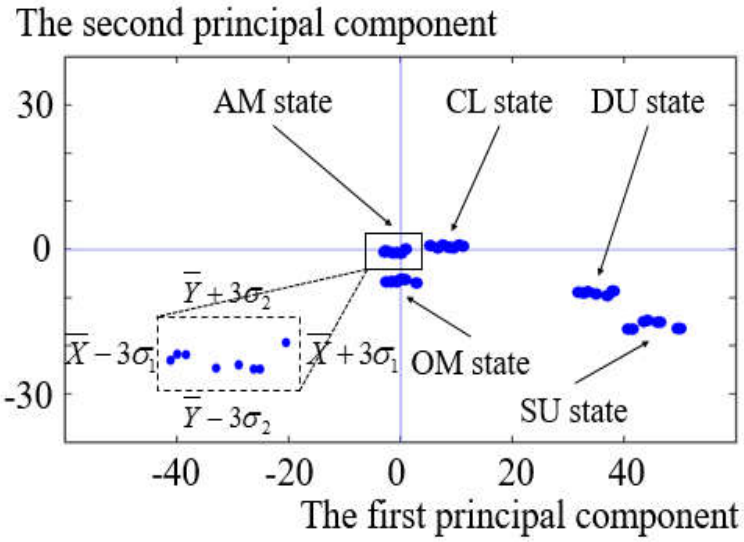

Fig. 66 Results of the Principal Component Analysis with the Angular Misalignment State as Reference

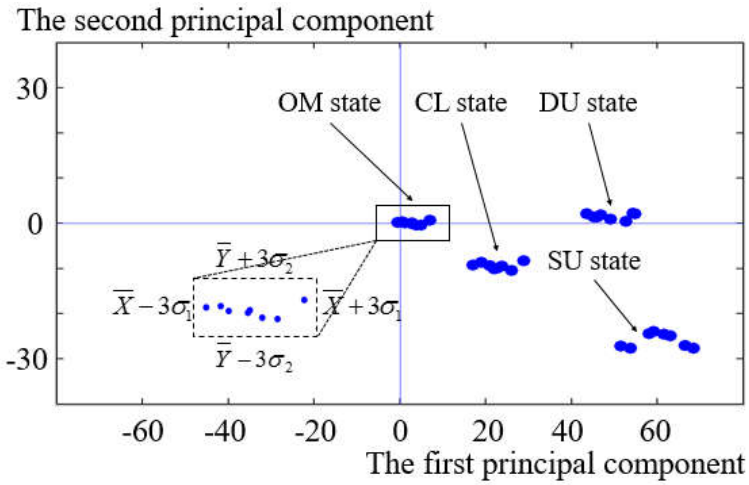

Fig. 67 Results of the Principal Component Analysis with the Offset Misalignment State as Reference

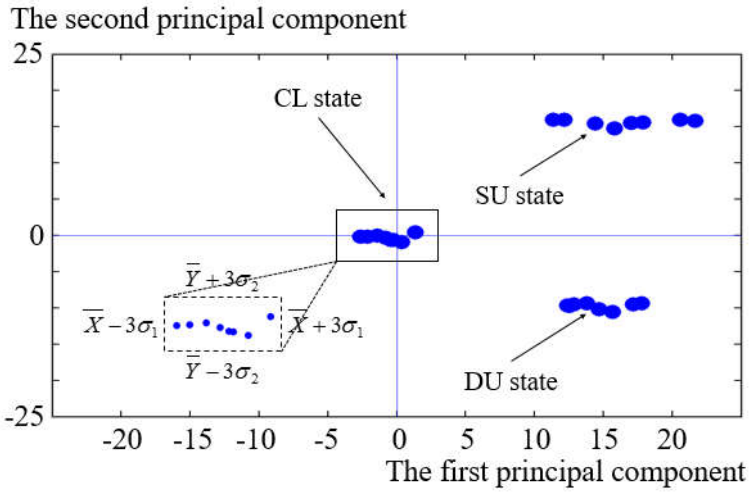

Fig. 68 Results of the Principal Component Analysis with the Loosening State as Reference

As shown in the figures above, the points representing the respective states are aggregated in the respective areas, and the identification of each diagnosed state can thus be realized. In this research, the calculation of the symptom parameters generally involves the use of a number of samples, and principal component analysis is performed for these parameters after rejecting the maximum and minimum values, with each sample corresponding to one point in the coordinate system. If the symptom parameters were not optimized, the points would fall into the respective areas chaotically, sometimes even appearing on the edge of the area, being mixed with points representing other states. In such case, miss-diagnosis may be resulted. Therefore, the afore-said LSM method was used to optimize the symptom parameters in order to distinguish more accurately the areas of different states for higher diagnosis accuracy.

Fig. 69 exhibits the example of the result of the principal component analysis that the area of reference state is mixed together with the area of other states, without the optimization using least square mapping. Fig. 70 exhibits the result of the principal component analysis after optimization using the least squares mapping. In this case, the values of the second principal component of samples in each state tend to be consistent, so that the area representing each state can be accurately distinguished to improve the accuracy of the diagnosis.

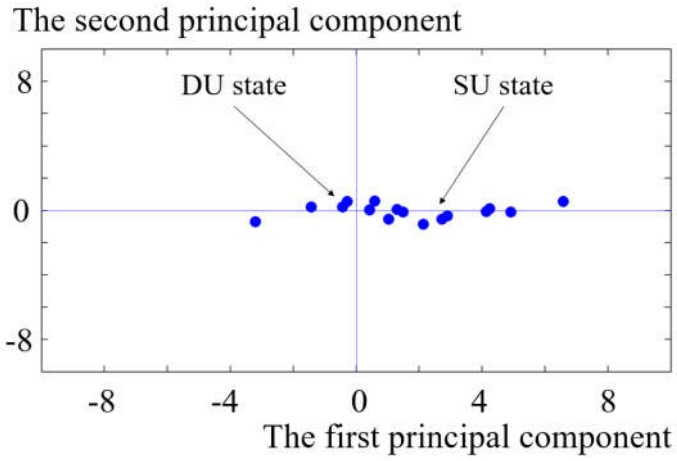

Fig. 69 Results of the Principal Component Analysis with the Normal State as Reference (Without Enhancing the Sensitivity of the Symptom Parameters with LSM)

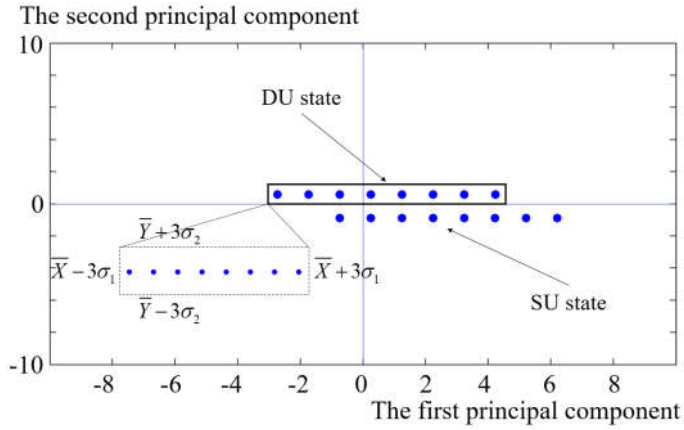

Fig. 70 Results of the Principal Component Analysis with the Loosening State as Reference (the Sensitivity of the Symptom Parameters Optimized with LSM)

4.7 Summary

This research has realized the integration of vibration acceleration signals measured at multiple positions and multiple directions based on the structural feature symptom parameters, and proposed the method to diagnose the structural faults of

rotating machinery (misalignment state, unbalanced state and loosening state) based on successive multivariate analysis. This method can realize the detection of structural faults of rotating machinery and the identification of types of anomalies. The validity of this methodology was confirmed by the experiment with the rotating machine simulator.

Future research will be targeted at the application of this method in field equipment diagnostics systems and the presentation of effective symptom parameters in the diagnosis of other types of anomaly states. Furthermore, relevant research will also be carried out on the prediction of remaining life after the determination of the anomaly state.

5. The precise diagnosis method of structural faults of rotating machinery based on combination of empirical mode decomposition and sample entropy and deep belief neural network (DBN)

Rotating machinery covers extensive mechanical equipment and plays an important role in industrial production. It generally serves in complicated and harsh environment, and may experience faults caused by environment [19]. It is of important significance to guarantee safe and reliable running of large rotating machinery.

Structural faults are the most common fault in rotating machinery. It not only causes direct baneful influences on performance of equipment and quality of products, but also it also causes excessive stress on surrounding components (such as bearings and gears) and causes secondary failure [20]. Therefore, early diagnosis of structural faults and diagnosis of fault types are extremely important subjects [21, 22]. Structural faults of rotating machinery often include unbalance, misalignment and looseness of fasteners which are caused by machinery structural defects. These structural faults lead to relatively low-frequency fault vibration. Compared with other types of faults, the faults caused by structural faults have two prominent common features, namely, component changes in the spectrum of vibration signal at the rotating frequency and its harmonic frequency. In particular, vibration signals of different structural faults under low-rotating speed present extremely similar characteristics on the frequency spectra, which bring a great difficulty to extraction of fault characteristics and diagnosis of fault types. Although some studies have revealed part of spectral characteristics of a series anomalous state, it is still insufficient to accurately draw a distinguishing line between different structural faults [23].

It is a common method in rotating machinery fault diagnosis to analyze fault vibration signals and disclose fault characteristics by effective signal processing technology [24, 25]. Whether key fault information can be extracted from vibration signals for diagnosis is an important challenge of signal processing technology. Traditional signal processing technologies covers analysis of time-domain signals and frequency-domain signals [26, 27]. They perform well in analysis of fault characteristics.

In frequency-domain analysis, characteristics of vibration signals in the frequency domain can be observed more easily by Fourier transform. In addition, explicit fault characteristics and diagnosis information can be acquired through frequency spectra of vibration signals [28]. However, signals of different types of fault caused by structural faults present extremely similar features on frequency spectra, especially under low rotating speed [29]. This increases the difficulty to extract fault characteristics and diagnosis of fault types significantly. The traditional frequency-domain analysis methods are unable to realize precise diagnosis of structural faults of such rotating machinery.

Compared with other machine faults, structural faults are prominent for changes of rotating frequency and changes of harmonic component. Moreover, vibration signals of structural faults are dynamic nonlinear system signals. Traditional time-domain analyses are mainly based on the hypothesis that the process of signal production is static and linear. Hence, they may make wrong judgment if fault signals are dynamic nonlinear systematic signals caused by structural faults [30, 31]. Some studies introduced empirical mode decomposition (EMD) in order to process these dynamic nonlinear systematic signals in rotating machinery fault. As a strong time-frequency analysis technology, EMD is an adaptive signal processing technology applicable to nonlinear and non-static process [32]. It has been widely used in many fields, including injection control, modeling, speech recognition, system control, etc. In many studies on EMD, EMD has been applied in fault diagnosis of rolling bearing, gears and rotors [33]. Nevertheless, these studies basically focus on one component of machineries rather than the type of fault [34]. It is necessary to emphasize on integrity of the equipment, but few have discussed the precise diagnosis method of rotating machinery structural faults. In addition, the original EMD method involves many problems, such as mode mixing, end effect, interpolation problem, end standards and optimal IMF selection [35]. These may make EMD produce meaningless or unnecessary intrinsic mode functions (IMFs), which may decrease the fault diagnosis accuracy and even misguide the diagnosis decision. It is necessary to further improve EMD or combine it with other processing techniques.

With the popularization of artificial neural network, fault diagnosis becomes more and more intelligent and accurate under the assistance of neural networks by its strong pattern recognition capability. Although some studies have implemented neural network-based fault diagnosis, the types of faults they can diagnose are specific fault states and are also very limited [36]. We have not found a literature that uses neural network to precisely diagnose structural faults, especially at low rotating speeds. Moreover, some studies focus on fault diagnosis of single part, instead of the global precise diagnosis of multiple fault types of multiple parts [37]. Other conventional discriminant methods like SVM have evident advantages in binary classification problems. However, SVM still fails to achieve precise diagnosis of structural faults, which is related with the difficult extraction of fault characteristics.

Deep learning possesses considerable advantages in pattern recognition and it has been highly used in many fields [38-41]. It makes the precise fault diagnosis based on deep learning, especially precise diagnosis of structural faults, possible. Appropriate processing of diagnosis signals before deep learning can further increase the diagnosis accuracy of machine faults [42]. In this study, diagnosis accuracy is too far from precise diagnosis when the original time-domain signals are input into the deep belief neural network (DBN). Although the diagnosis accuracy is increased significantly by inputting the frequency-domain signals, the diagnosis accuracy under low rotating speed is still insufficient to meet requirements on precise diagnosis. In order to increase accuracy of precise diagnosis, the fault information extraction method that combines EMD and sample entropy was proposed. The original signal is decomposed into many intrinsic mode functions with different frequency domains, and the sample entropy is calculated for extracting the signals that carry fault information with high SNR. The extracted fault signal is reconstructed into a new vibration signal that will carry abundant fault information. The reconstructed signal as treated the input and brought satisfying diagnosis accuracy under different rotating speeds, meeting the requirements of precise diagnosis. Structural faults of rotating machinery could be recognized by this method. On this basis, an intelligent diagnosis system for structural faults could be constructed.

In this study, the precise diagnosis method based on the fault information extraction method that combines EMD and sample entropy as well as the DBN was introduced firstly. Next, validity of this method was verified by an experiment. Finally, the diagnosis results of this method were compared with those of other methods. Its superiorities to other diagnosis methods were discussed and verified. Procedure of the proposed method is shown in Fig. 71 and includes the following steps:

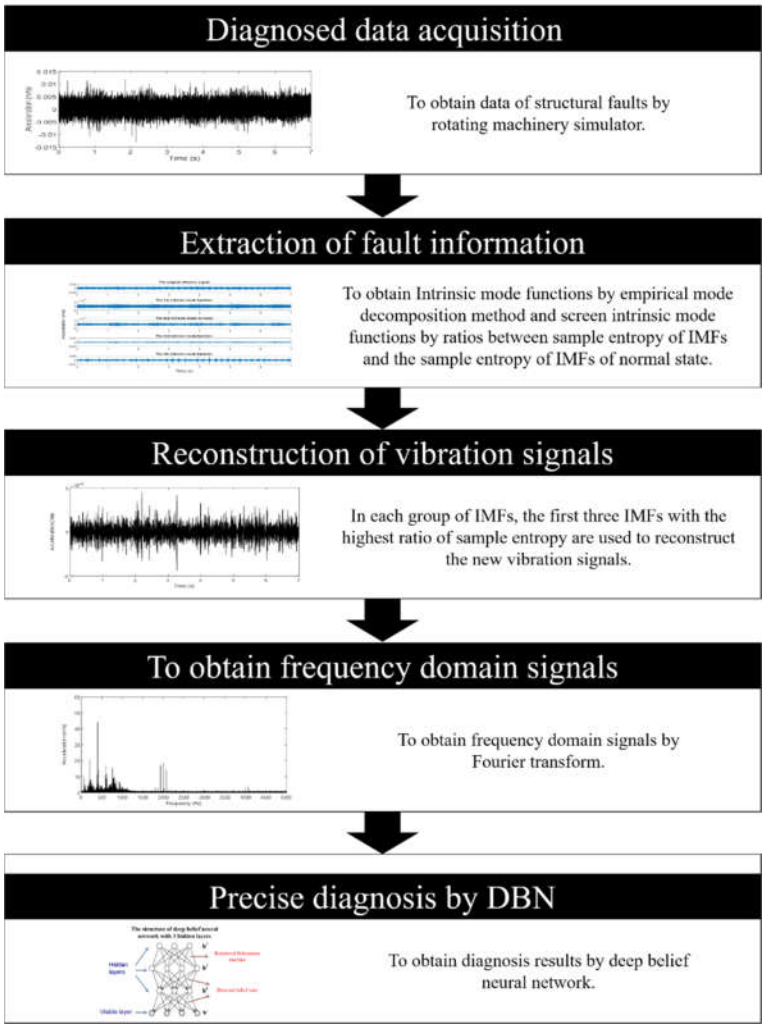

Fig. 71 Precision diagnostic process based on deep belief neural networks

1. measuring vibration signals of the targeted rotating machinery (hereinafter referred as the diagnosed signals);

2. decomposing the original vibration signal into several IMFs by EMD;

3. calculating sample entropy of IMFs and screen the signals that contain many fault information;

4. reconstructing the screened signals into new characteristic signals;

5. implementing FFT to new characteristic signals, and then gain their frequency-domain characteristic signals; and

6. inputting the frequency-domain characteristic signals into the trained DBN and get the final diagnosis results.

5.1 Extraction of fault information

Fault information in diagnosed signals shall be extracted before the training and use of the DBN in order to increase diagnosis accuracy based on DBN. This can be realized by combining EMD and sample entropy.

5.1.1 Empirical mode decomposition

EMD (Empirical mode decomposition) is an adaptive signal analysis and processing technique. In fact, it makes stationary processing of data sequences or signals. EMD has evident advantages in processing non-stationary and nonlinear data and has high SNR. Since vibration signals of different structural faults often have many similar characteristics on the waveform and frequency spectra, it is difficult to distinguish different types of structural faults. To extract fault information and improve the diagnosis accuracy, the diagnosed signal was decomposed into several IMFs by EMD.

Instantaneous frequency at any one point of IMFs is meaningful. At any moment, signals can contain several IMFs. Composite signals are formed when IMFs overlap mutually.

The decomposition process is introduced as follows:

Effective EMD process of one given signal $x(t)$ contains the following steps:

(1) Find out all extreme points of the original signal $x(t)$, including the maximum point $(xmax(t))$ and the minimum point $(xmin\ (t))$.

(2) Form the lower envelope $emint(t)$ of the minimum point and the upper envelope of maximum point $emax(t)$ by using the interpolation method.

(3) Calculate the mean $m(t)=(emint(t)+emax(t))/2$.

(4) Draw the details $d(t)=x(t)-m(t)$.

(5) If *d(t)* has a negative local maximum and a positive local minimum, it is not an IMF and screening shall be continued. In other words, all extreme points of *d(t)* shall be recognized and all above steps shall be repeated until meeting the given standards. If the screening process is accomplished successfully, the first IMF is extracted and it shall be subtracted from the original data. Next, repeat this process to get the next IMF until all IMFs are extracted.

5.1.2 Sample entropy

Each diagnosed signals can decompose several IMFs by the above EMD. However, only several signals that contain many fault information have to be screened and reconstructed into new vibration signals for precise diagnosis. This was accomplished by sample entropy in this study.

Sample entropy *(SampEn)* is an improved method to measure complexity of time sequence based on *(ApEn)*. It has been used in assessment of complexity of physiological time series and diagnosis of pathological state. In this study, sample entropy can be used as the standard to judge how much fault information that each signal contains.

The calculation process of sample entropy is introduced as follows:

The original data is set as a time series with a length of N, which is expressed as {u(i):1≤i≤N}.

(1) Construct a group of m-dimensional vectors: *X(1),X(2),…,X(N-m+1)*, and where *X(i)={u(i),u(i+1),…,u(i+m)}*.

(2) The distance *d[X(i),X(j)]* between vectors *X(i)* and *X(j)* as the one with the maximum difference in corresponding elements is:

$$d\left[X(i),X(j)\right]=\max_{k=0\sim m-1}\left|u(i+k)-u(j+k)\right| \tag{46}$$

(3) For each *{i:1≤i≤N-m+1},* a statistics on number of *d[X(i),X(j)]<r* is carried out when the allowable deviation is r, which is recorded as *Nm(i)*. Meanwhile, the ratio between *Nm(i)* and the total distance is calculated, which is denoted as:

$$C_i^m\left(r\right)=N_m(i)/\left(N-m\right) \tag{47}$$

(4) Calculate the mean of all *i*, which is denoted as:

$$\phi^m\left(r\right)=1/\left(N-m\right)\sum_{i=1}^{N-m}C_i^m\left(r\right) \tag{48}$$

(5) Increase the dimension m by *1* to *m+1*. Repeat Steps (1) ~ (4) to get:

$$C_i^{m+1}(r) = N_{m+1}(i) / (N - m + 1) \tag{49}$$

$$\varphi^{m+1}(r) = \frac{1}{N-(m+1)} \sum_{i=1}^{N-(m+1)} C_i^{m+1}(r) \tag{50}$$

(6) Theoretically, the sample entropy *SampEn(N,m,r)* of this series is:

$$SampEn(m,r) = \lim_{N\to\infty} \left\{ -1\mathrm{n}\left[\varphi^{m+1}(r) / \varphi^{m}(r) \right] \right\} \tag{51}$$

Practically, N cannot be ∞. When N is a limited value, it is estimated that:

$$SampEn(N,m,r) = -1\mathrm{n}\left[\varphi^{m+1}(r) / \varphi^{m}(r) \right] \tag{52}$$

According to the calculated value of sample entropy, the signal with the maximum sample entropy is used as the input of neural network.

Since sample entropy is an index that mainly assesses the complexity of the signal, it is inadequate to extract essential fault information for precise diagnosis. For effective extraction of fault information, the sample entropies of different IMFs which are decomposed by EMD method from both the diagnosed signal and the normal state signal have to be calculated. The ratio between IMFs of diagnosed signal and IMFs of the normal state signals was used as the reference to screen the signal containing many fault information.

5.1.3 The reconstruction of extracted fault signal

Through the empirical modal decomposition above, the original vibration signal is decomposed into several intrinsic mode functions. Each intrinsic mode function contains varying degrees of fault information. IMFs that contain many fault information can be screened by the sample entropy. New vibration signals can be reconstructed by integrating these IMFs. The new signals have higher SNR than the original vibration signal and can increase the diagnosis accuracy effectively. In this study, the first three IMFs with the highest sample entropy ratios (farther from 1) were chosen from each group to reconstruct the new signals. New signals were used to replace the original vibration signal in precise diagnosis. The extraction of fault information and the reconstruction of the vibration signal are shown in Fig. 72. The reconstructed signals are shown in Fig. 73.

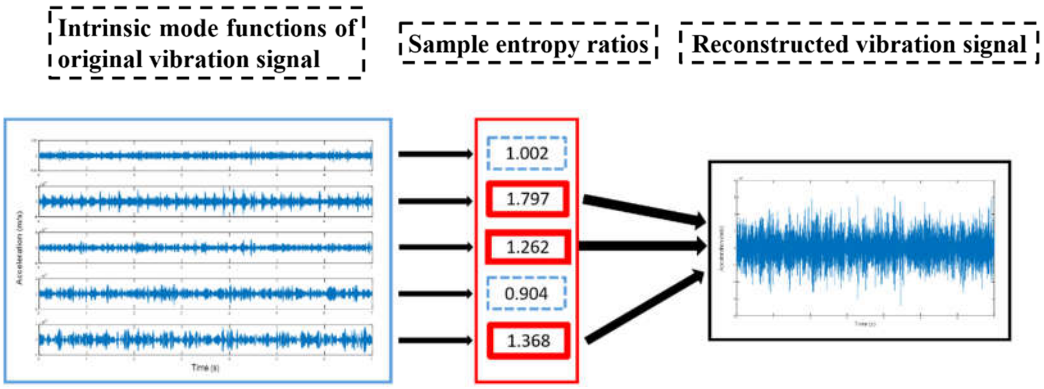

Fig. 72 The process of extraction of fault information and reconstruction of extracted fault signal

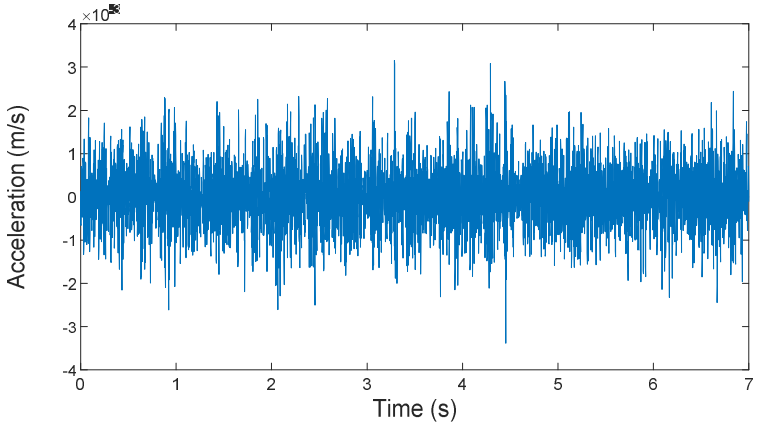

Fig. 73 Reconstructed vibration signal (300 rpm, unbalanced state)

5.2 Structure and principle of DBN

DBN is a probability generation model and a multi-hidden layer neural network formed by multiple restricted Boltzmann machines (RMB). DBN model can extract features layer by layer from the original data through layered piling of RBM, thus getting high-level expressions. The core of DBN is to optimize connection weight of deep neural network by using the layer greedy learning algorithm [43, 44]. Firstly, characteristics in data shall be mined effectively by unsupervised layer-wise training. Secondly, classification ability of DBN shall be optimized by the reverse supervised fine adjustment based on adding the corresponding classifiers.

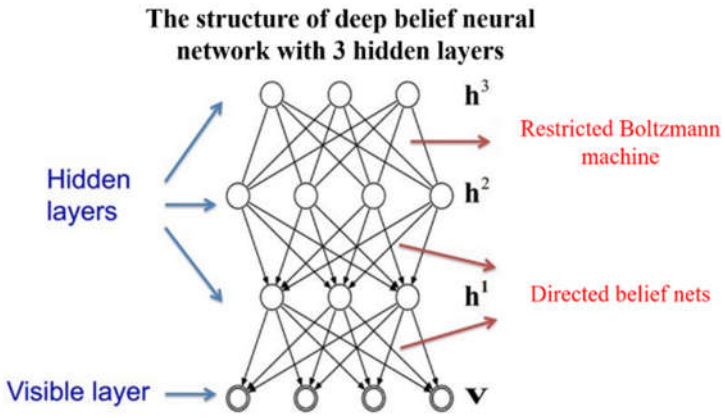

Fig. 74 Structure of the deep belief neural network with three hidden layers

DBNs are composed of multiple RMBs. The structure of one DBN is shown in Fig. 74. This is "restricted" into one visible layer and multiple hidden layers. There are connections between layers, but there's no connection between units in each layer [45]. Units in hidden layers were trained to capture characteristics of input data in the visible layer. RBM is a neural sensor composed of one explicit layer and one hidden layer. Neurons between the explicit layer and the hidden layer adopt two-way full connections. Three RBMs were "connected in series" from the bottom to up, so the DBN in Fig. 74 was constructed. The hidden layer of the first RBM is the explicit layer of the second RBM, and the output of the second RBM is the input of the third one. During training, RBM of the current layer can only be trained after the previous layer of RMB has been trained completely. This shall be implemented until the last layer. The structure of RBM is shown in Fig. 75.

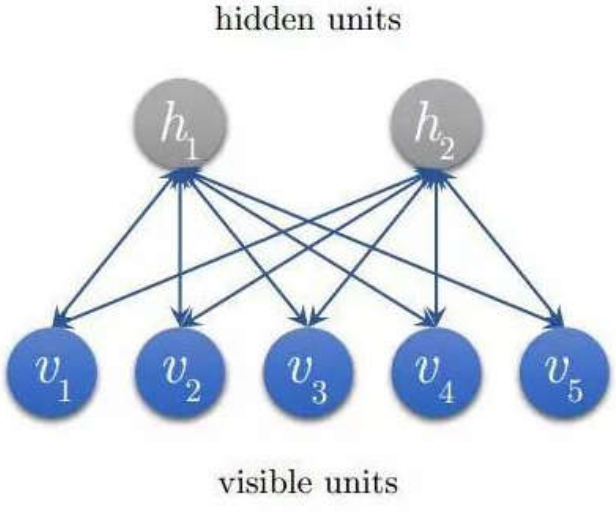

Fig. 75 The structure of RBM (Restricted Boltzmann Machine)

To train the DBN, unsupervised pre-training based on RBM was performed firstly. Weights were initialized by the comparison divergence algorithm, followed by supervised optimized training. During supervised optimized training, it has to get a certain output from the input by using the forward propagation algorithm. Next, weights and offsets of the network shall be updated by the backward propagation algorithm. The training process of DBN is shown as follows. When training DBN, a layer-by-layer unsupervised method is used to learn the parameters. As shown in Fig. 76, first, the data vector x and the first hidden layer are treated as one RBM, and the parameters of the RBM (the weights of x and h1, the offset of each node of x and h1, etc.) are trained, and then fixed. By treating h1 as the visible vector, h2 as the hidden vector, and training the second RBM, the parameters of RBM can be obtained and then fixed. Afterwards, the RBM composed of h2 and h3 is trained.

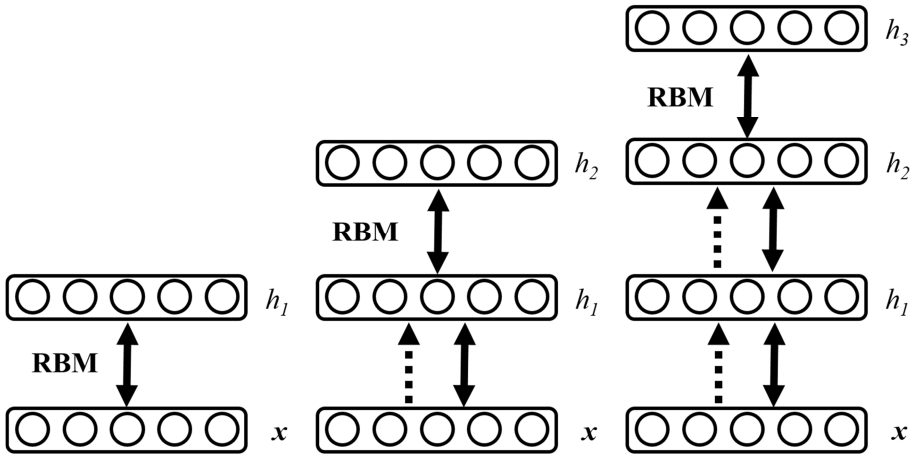

Fig. 76 The training process for the Deep Belief Network (DBN)

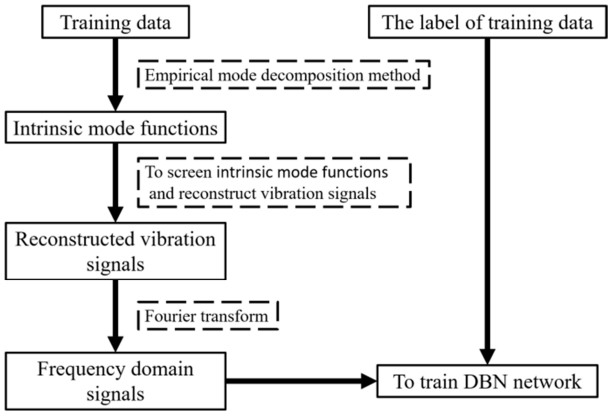

Fig. 77 The training for the proposed model

The training process of DBN is shown as follows. EMD was performed to experimental data under different states (labels). Signals containing abundant fault information were screened according to sample entropy and then reconstructed into new

vibration signals. Frequency spectra and labels of these reconstructed signals to train the neural network. EMD was performed to experimental data under different states (labels). Signals containing abundant fault information were screened according to sample entropy ratio and then reconstructed into new vibration signals. Frequency spectra and labels of these reconstructed signals were used to train the neural network. The training for the proposed model is shown in Fig. 77.

5.3 Precise diagnosis of structural faults of rotating machinery

In this chapter, the proposed method was used to precise diagnosis of structural faults of rotating machinery. Firstly, vibration signals of different structural faults shall be collected (Fig. 78). The following procedure was repeated during collection of vibration signals under each state.

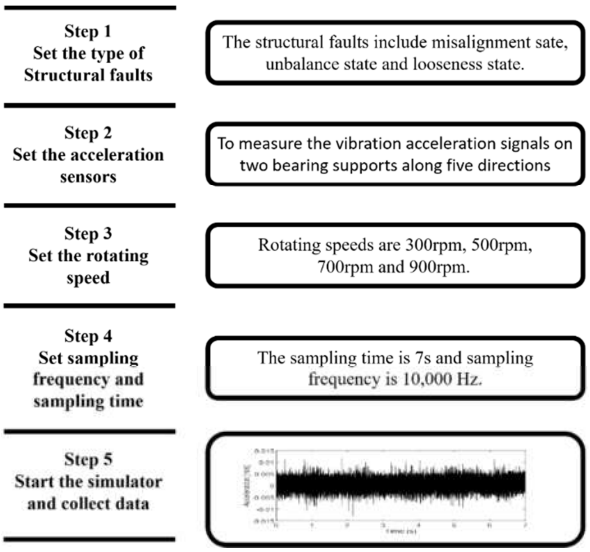

Fig. 78 The process of signal collection

The rotating machinery simulator in Fig. 79 was used to reproduce structural faults of rotating machinery. The layout of acceleration sensors is shown in Fig. 80. They measured the vibration acceleration signals on two bearing supports along five directions (left vertical direction, right vertical direction, left horizontal direction, right horizontal direction and axial direction).

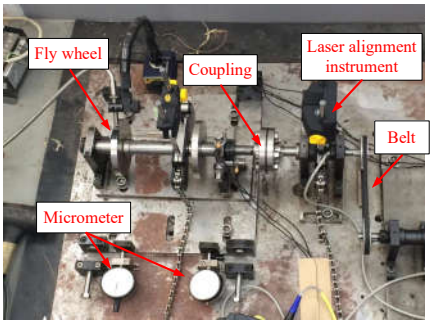

(a) Rotating machinery simulator (b) Laser alignment instrument

Fig. 79 Rotating machinery simulator and laser alignment instrument

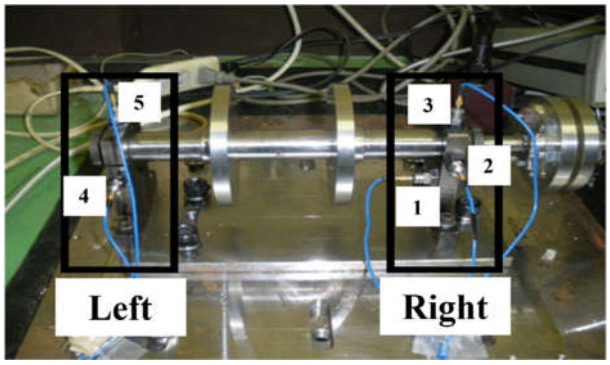

Fig. 80 The layout of acceleration sensors

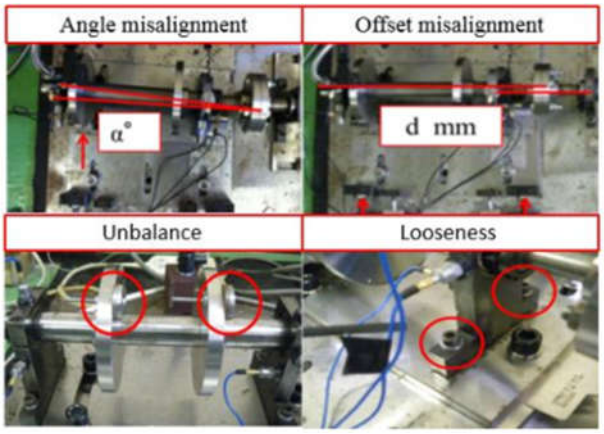

Fig. 81 Set each structure faults status on the rotating machinery simulator

It can be seen from Fig. 81 that the preset structural faults include misalignment state (angular misalignment and offset misalignment), unbalance state and looseness state (loosing of pedestal and bearing pedestal). The misalignment state can be set by adjusting the position and angle of the spindle through the assistant positioning of shaft laser alignment meter. The unbalance state was set by configuring different weights through the flange plate. The looseness state could be set by adjusting the tightness of bolts on the bearing box and pedestal.

5.4 Extraction results of characteristic signals

In this study, the measured rotating speeds are 300, 500, 700, and 900 rpms, respectively. Acceleration sensors are used to measure the vibration signal in 5 directions. The vibration signal is stored by the data collector and converted into csv format for subsequent processing. The sampling frequency is 10,000 Hz, the sampling time is 7 s, and the data length is 70,000. The original vibration signals and the EMD results are shown in Fig. 82~Fig. 85.

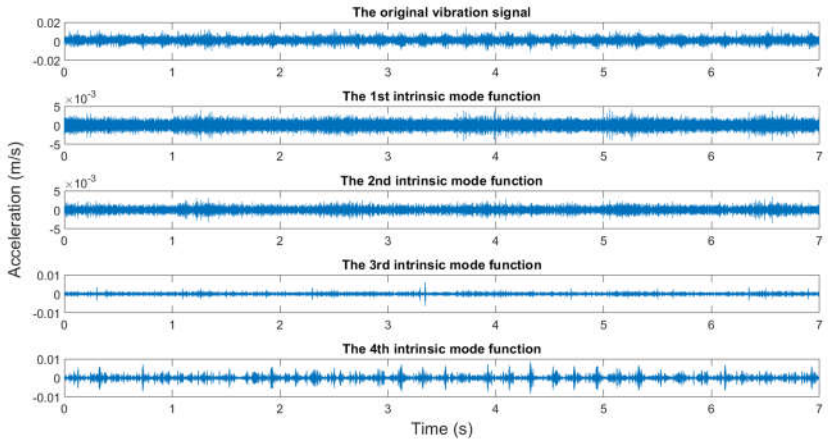

Fig. 82 The original vibration signals and the EMD results (300 rpm, the looseness state of the pedestal)

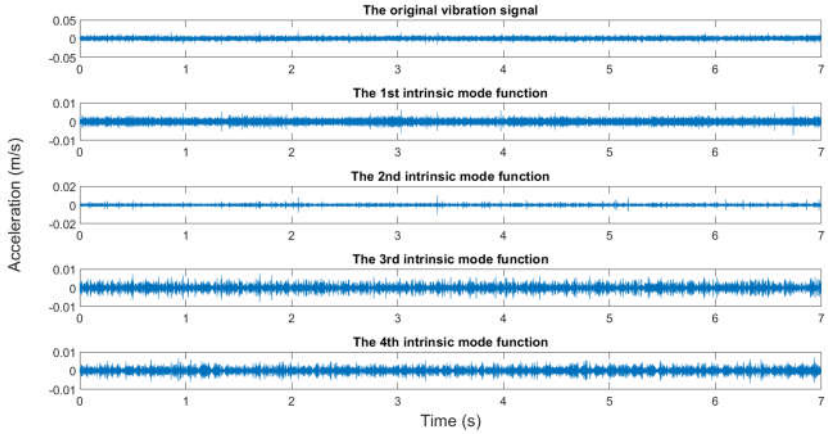

Fig. 83 The original vibration signals and the EMD results (500 rpm, the looseness state of the bearing housing)

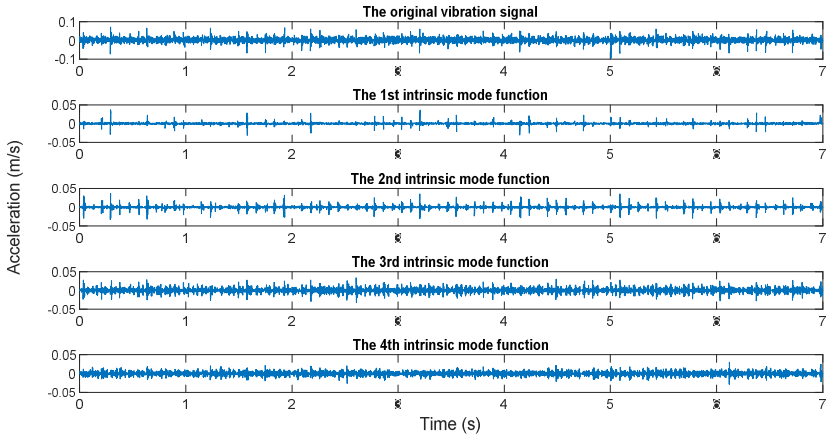

Fig. 84 The original vibration signals and the EMD results (700 rpm, unbalanced state)

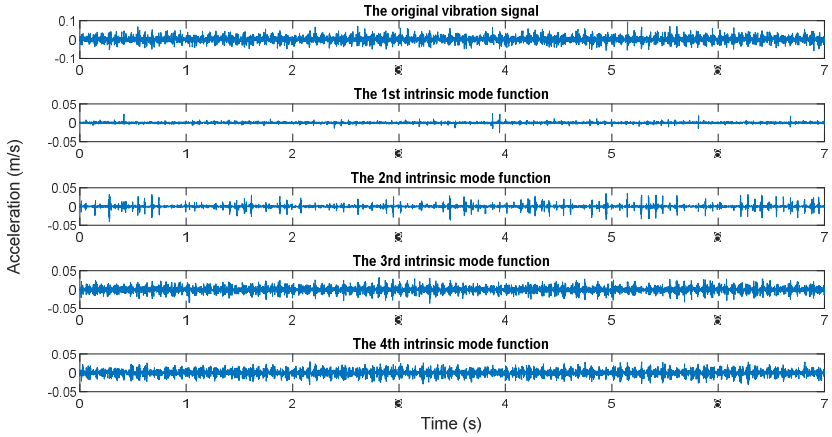

Fig. 85 The original vibration signals and the EMD results (900 rpm, misalignment state)

It generally can be concluded from EMD results that the first IMFs among 5 decomposed IMFs have relatively dense images and may contain abundant fault characteristics, while the rest IMFs have relatively sparse images and may contain few fault characteristics. However, this was inadequate to screen signals containing abundant fault information. To screen signals containing many fault information, sample entropy of each IMF shall be calculated.

Parameters were set as follows before calculating the sample entropy: the dimension m and threshold r of the constructed samples were m=2500 and r=0.008, respectively. Due to the size of mass data in the original signal, it took a considerable long time to calculate sample entropy. In this study, 5000 sample points in the original signal were selected to calculate sample entropy, which could increase the calculation efficiency and shorten calculation time significantly. The ratio between sample entropy of IMFs of different structural fault and the sample entropy of IMFs of normal state can be expressed as:

Table 1 Ratios between sample entropy of IMFs and the sample entropy of IMFs of normal state (300 rpm, the looseness state of the pedestal)

The numbering of intrinsic mode function	The ratio with the sample entropy of reference state
1	1.006
2	1.006
3	1.006
4	1.003
5	0.380
6	1.314
7	1.248
8	1.004
9	1.004
10	1.004

Table 2 Ratios between sample entropy of IMFs and the sample entropy of IMFs of normal state (500 rpm, the looseness state of the bearing housing)

The numbering of intrinsic mode function	The ratio with the sample entropy of reference state
1	1.006
2	1.006
3	1.006
4	1.159
5	0.766
6	1.900
7	0.484
8	1.516
9	1.004
10	1.004

Table 3 Ratios between sample entropy of IMFs and the sample entropy of IMFs of normal state (700 rpm, unbalanced state)

The numbering of intrinsic mode function	The ratio with the sample entropy of reference state
1	1.006
2	1.006
3	1.006
4	1.006
5	0.376
6	0.642
7	0.866
8	0.964
9	1.442
10	0.741

Table 4 Ratios between sample entropy of IMFs and the sample entropy of IMFs of normal state (900 rpm, misalignment state)

The numbering of intrinsic mode function	The ratio with the sample entropy of reference state
1	1.006
2	1.006
3	1.006
4	1.006
5	0.400
6	1.973
7	0.985
8	0.690
9	1.326
10	0.778

In each group of IMFs, the first three IMFs with the highest ratio of sample entropy were used to reconstruct the new vibration signals:

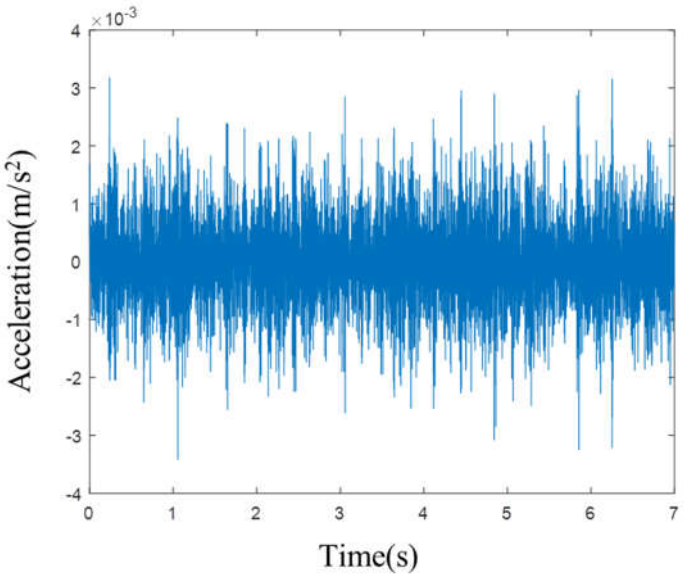

Fig. 86 Reconstructed vibration signal (300 rpm, the looseness state of the pedestal)

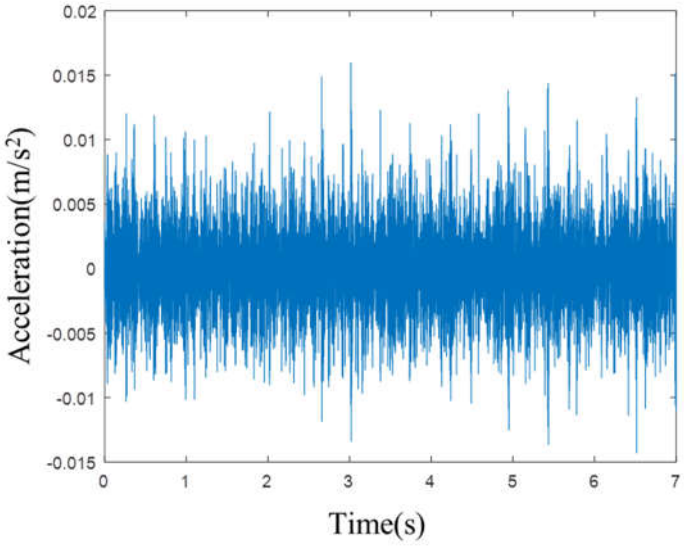

Fig. 87 Reconstructed vibration signal (500 rpm, the looseness state of the bearing housing)

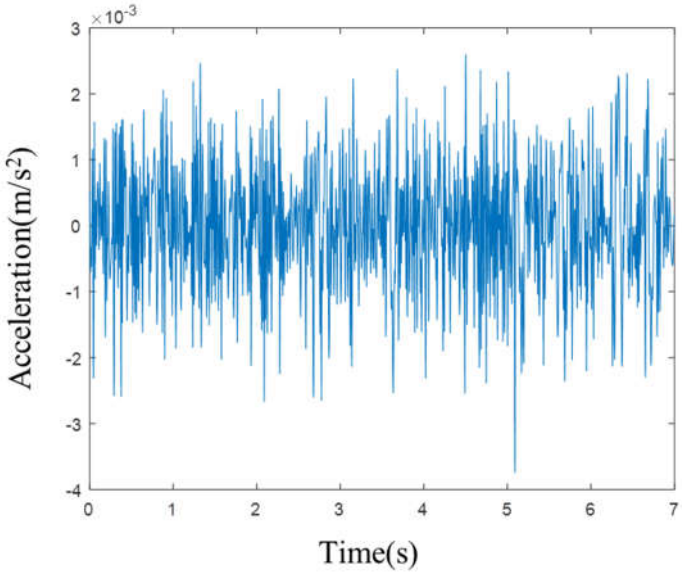

Fig. 88 Reconstructed vibration signal (700 rpm, unbalanced state)

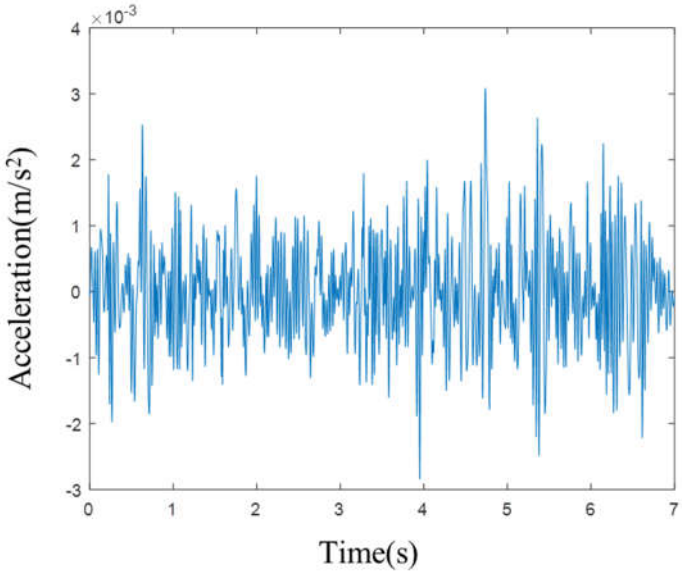

Fig. 89 Reconstructed vibration signal (900 rpm, misalignment state)

Compared with the original vibration signal, the reconstructed vibration signals had fewer impacts from noises in view of images, and higher proportion of fault information. Diagnosis based on reconstructed vibration signals can further increase accuracy of precise diagnosis.

5.5 Diagnosis results based on DBN

To verify validity of the proposed method, diagnosis results based on time-domain signal, diagnosis results based on frequency-domain signal, and diagnosis results based on combination of frequency-domain signals and fault information extraction method

were compared.

Firstly, parameters of the neural network were set uniformly:

1. DBN size was set 100-50 (the explicit layer had 100 neurons and the hidden layer had 50 neurons).

2. The number of iteration for samples was 100.

3. The batch size was 10.

4. Learning rate was 0.01.

When only time-domain signals were used in diagnosis:

Table 5 Diagnostic results using time domain signals

The type of diagnostic data	Rotating speed	Diagnostic accuracy
Time domain signal	300rpm	20%
Time domain signal	500rpm	20%
Time domain signal	700rpm	20%
Time domain signal	900rpm	20%

Table 5 showed that the diagnosis accuracy was very low under low-rotating speeds and it was difficult to realize precise diagnosis of structural faults when the diagnosed signals were time-domain signals. Based on above analysis, structural faults have prominent characteristics, that is, changes of the rotating frequency and its harmonic component. This indicates that fault characteristics were mainly reflected on frequency-domain signals. As a result, it is difficult to extract and learn fault characteristics when using time-domain signals only in diagnosis. The diagnosis accuracy is low accordingly.

When only frequency-domain signals were used in diagnosis:

Table 6 Diagnostic results using frequency domain signals

The type of diagnostic data	Rotating speed	Diagnostic accuracy
Frequency domain signal	300rpm	80%
Frequency domain signal	500rpm	82%
Frequency domain signal	700rpm	98%
Frequency domain signal	900rpm	96%

When the diagnostic signal was a frequency domain signal, the diagnostic accuracy is very high at high rotating speeds (700 rpm and 900 rpm), but the accuracy of the precision diagnosis is very low at low rotating speeds (300 rpm and 500 rpm). According to above analysis, the most prominent common features of structural faults are changes of rotating frequency and its harmonic components. Different types of

structural faults have very similar characteristics, especially under low rotating speed. Therefore, the diagnosis accuracy based on frequency-domain signals was not satisfying under low rotating speed although the overall diagnosis accuracy was improved significantly. Fault characteristics have to be further extracted and SNR of signals shall be increased in order to further increase the diagnosis accuracy.

After fault information were extracted and vibration signals were reconstructed, frequency-domain signals were used in diagnosis:

Table 7 Diagnostic results using frequency domain signals after extracting fault characteristics

The type of diagnostic data	Rotating speed	Diagnostic accuracy
Frequency domain signal after extracting fault features	300rpm	100%
Frequency domain signal after extracting fault features	500rpm	100%
Frequency domain signal after extracting fault features	700rpm	99%
Frequency domain signal after extracting fault features	900rpm	100%

During EMD processing of diagnosed signals, IMFs that contain abundant fault information were chosen according to the ratio with sample entropy of normal state and they were reconstructed into new vibration signals. The frequency-domain signals of these new vibration signals were used in diagnosis, which achieved very high accuracy under both high and low rotating speeds. The precise diagnosis was realized.

This method can increase diagnosis accuracy significantly and realize precise diagnosis of structural faults. This is because reconstructed vibration signals not only extract fault characteristics in original signals effectively, but also have extremely high SNR which is conducive to increase diagnosis accuracy greatly. The diagnosis accuracy was verified by changing parameters of DBN.

1. DBN size was set 100-75 (the explicit layer had 100 neurons and the hidden layer had 75neurons).

2. The number of iteration for samples was 50.

3. The batch size was 20.

4. Learning rate was 0.05.

Diagnosis results:

Table 8 Diagnostic results using frequency domain signals after extracting fault characteristics

(Changing the parameters of DBN)

The type of diagnostic data	Rotating speed	Diagnostic accuracy
Frequency domain signal after extracting fault features	300rpm	100%
Frequency domain signal after extracting fault features	500rpm	100%
Frequency domain signal after extracting fault features	700rpm	99%
Frequency domain signal after extracting fault features	900rpm	100%

1. DBN size was set 100-100 (the explicit layer had 100 neurons and the hidden layer had 75neurons).

2. The number of iteration for samples was 50.

3. The batch size was 10.

4. Learning rate was 0.05.

Diagnosis results:

Table 9 Diagnostic results using frequency domain signals after extracting fault characteristics

(Changing the parameters of DBN)

The type of diagnostic data	Rotating speed	Diagnostic accuracy
Frequency domain signal after extracting fault features	300rpm	100%
Frequency domain signal after extracting fault features	500rpm	100%
Frequency domain signal after extracting fault features	700rpm	99%
Frequency domain signal after extracting fault features	900rpm	100%

It can be known from above diagnosis results that the proposed method still maintains extremely high diagnosis accuracy after parameters of DBN are changed. This method can adjust parameter settings according to different needs and realize precise diagnosis.

5.6 The comparison with diagnostic results of diagnostic methods based on traditional neural network

5.6.1 Common characteristic parameters

In order to compare the diagnostic accuracy of the precision diagnostic method with the diagnostic methods which based on other neural network, it is necessary to extract the fault characteristics for precise diagnosis before using the traditional neural network for diagnosis. Dimensional and dimensionless symptom parameters are capable of extracting the characteristics of vibration signals and are commonly used for mechanical condition monitoring. These parameters allow for more sensitive detection of mechanical faults and for distinguishing fault types [46]. However, how to extract symptom parameters and whether the extracted symptom parameters are suitable for diagnosis has always been an important issue. In this study, reference is made to some of the symptom parameters proposed in the relevant research, as well as the symptom parameters commonly used in statistics, which will be used in the diagnostic method based on traditional neural network [47, 48].

The 14 characteristic parameters are defined as follows.

Assumed that the measured time domain vibration signal x_i $(i = 1 \sim N)$ has N points.

Average value:

$$\bar{x} = \frac{\sum_{i=1}^{N} x_i^2}{N} \tag{53}$$

Standard variance:

$$\sigma = \sqrt{\frac{\sum_{i=1}^{N} (x_i - \bar{x})^2}{N-1}} \tag{54}$$

Valid value:

$$p_1 = \frac{\sum_{i=1}^{N} x_i^2}{N} \tag{55}$$

Peak:

$$p_2 = \frac{\sum_{i=1}^{N_p} \overline{|x_i|}_p}{N_p} \tag{56}$$

Skewness:

$$p_3 = \left| \frac{\sum_{i=1}^{N} \left(x_i - \bar{x}\right)^3}{\sigma^3} \right| \tag{57}$$

Kurtosis:

$$p_4 = \frac{\sum_{i=1}^{N} \left(x_i - \bar{x}\right)^4}{\sigma^4} \tag{58}$$

Crest factor:

$$p_5 = p_2 / \sigma \tag{59}$$

Peak skewness:

$$p_6 = \left| \frac{\sum_{i=1}^{N} \left(x_{pi} - \overline{x_p}\right)^3}{\sigma_p^{\,3}} \right| \tag{60}$$

Peak kurtosis:

$$p_7 = \left| \frac{\sum_{i=1}^{N} \left(x_{pi} - \overline{x_p}\right)^4}{\sigma_p^{\,4}} \right| \tag{61}$$

Average frequency:

$$\bar{f} = \frac{\sum_{i=1}^{I} f_i \cdot F(f_i)}{\sum_{i=1}^{I} F(f_i)} \tag{62}$$

Standard deviation of the spectrum:

$$\sigma = \sqrt{\frac{\sum_{i=1}^{I} (f_i - \bar{f})^2 \cdot F(f_i)}{I}} \tag{63}$$

Index of waveform stability:

$$p_9 = \frac{\sum_{i=1}^{I} f_i^2 \cdot F(f_i)}{\sqrt{\sum_{i=1}^{I} F(f_i) \sum_{i=1}^{I} f_i^4 \cdot F(f_i)}} \tag{64}$$

Geometric mean of the spectrum:

$$p_{10} = \sqrt[I]{\prod_{i=1}^{I} F(f_i)} \tag{65}$$

Arithmetic average of the spectrum:

$$p_{11} = \sum_{i=1}^{I} F(f_i) / I \tag{66}$$

5.6.2 Diagnostic method based on back propagation neural network

BP neural network (back propagation neural network) is the most common kind of neural network. It is a multi-layer feedforward network trained by error back propagation. The algorithm is called BP algorithm, the basic idea is gradient descent method. Gradient search technology is used to minimize the error mean square error between the actual output value of the network and the expected output value [49]. In this study, the symptom parameters and their principal components are used as inputs to the BP neural network respectively. The model of the traditional bp neural network is shown as below:

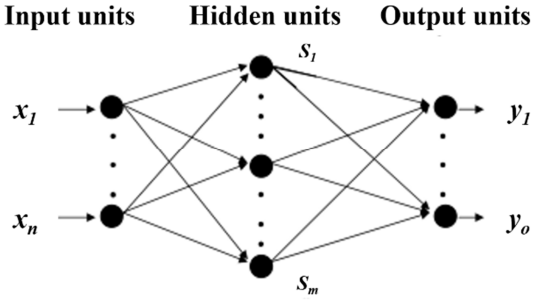

Fig. 90 Three-layer BP neural network consisting of input layer, hidden layer and output layer

The basic BP algorithm includes two processes of forward propagation of signals and back propagation of errors. That is, the calculation of the input error is performed in the direction from the input to the output, and the adjustment of weight and threshold are performed from the output to the input. In the case of forward propagation, the input signal acts on the output node through the hidden layer and undergoes a nonlinear

transformation to generate an output signal. If the actual output does not match the expected output, it is transferred to the backpropagation process of the error. Error back propagation is to pass the output error back to the input layer through the hidden layer, and distribute the error to all the units in each layer. The error signal obtained from each layer is used as the basis for adjusting the weight of each unit. By adjusting the connection strength between the input node and the hidden layer node and the connection strength and threshold of the hidden layer node and the output node, the error is decreased along the gradient direction. After repeated learning training, when the network parameters (weights and thresholds corresponding to the minimum error) are determined, the training will stop. We can think of the network as a pattern recognition tool with tunable parameters that have been trained under supervision, ie a given set of input-output combinations has been presented. For most architectures, these tunable parameters are expressed in the form of weight w.

In this study, the characteristic parameters and their principal components are used as inputs to the BP neural network respectively. The results of the diagnosis are as follows:

Table. 10 Diagnostic results of back propagation neural network

The type of diagnostic data	Rotating speed	Diagnostic accuracy
Symptom parameters	300rpm	16%
Symptom parameters	500rpm	16%
Symptom parameters	700rpm	23%
Symptom parameters	900rpm	18%
Principal component	300rpm	17%
Principal component	500rpm	11%
Principal component	700rpm	16%
Principal component	900rpm	12%

From the table above, we can know that the diagnostic accuracy based on the BP network at each rotational speed is very low regardless of whether the characteristic parameters or the principal components of the characteristic parameters are used for diagnosis. BP neural network is difficult to learn all the fault features because of its relatively simple structure. It is difficult to meet the requirements of precision diagnosis using BP neural network-based diagnostic methods.

5.6.3 Diagnostic method based on convolutional neural network

Convolutional neural network is a multi-layer feedforward neural network. It is good at dealing with related machine learning problems of images [50], especially large images. It has excellent performance for large image processing and is widely used in image recognition. Through a series of methods, the convolutional network has successfully reduced the image recognition problem with huge data volume and finally enabled it to be trained. It includes convolutional layers and pooling layers. The traditional cnn neural network is shown below:

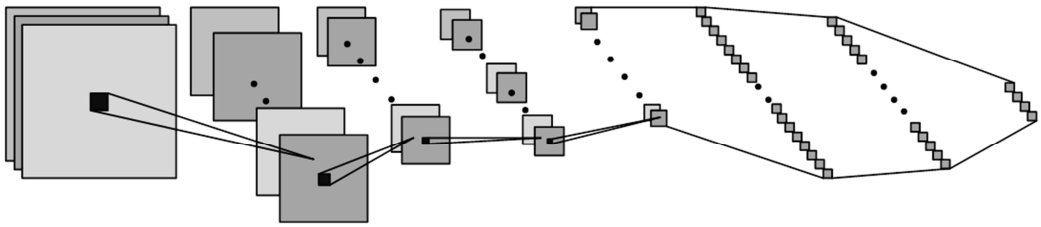

Fig. 91 The structure of traditional CNN neural network

This is the most typical convolutional network, consisting of convolutional layers, pooled layers, and fully connected layers. Four of the main operations include:

1. Convolution;
2. Nonlinear processing;
3. Pooling or subsampling;
4. Classification.

In this study, the characteristic parameters and principal components are reconstructed into a matrix of image forms and then used as input to convolutional neural network. When the characteristic parameters are used as input, each state signal is divided into 12 segments, and a set of special feature parameters can be calculated according to each segmentation signal. The number of each group of feature parameters is 12. The characteristic parameters are rearranged and constructed into a 12×12 new pixel matrix as an input to the CNN neural network. Similarly, when the principal component is used. The results of the diagnosis are as follows:

Table. 11 Diagnostic results of convolutional neural network

The type of diagnostic data	Rotating speed	Diagnostic accuracy
Symptom parameters	300rpm	70%
Symptom parameters	500rpm	70%
Symptom parameters	700rpm	80%
Symptom parameters	900rpm	99%
Principal component	300rpm	70%
Principal component	500rpm	80%
Principal component	700rpm	80%
Principal component	900rpm	99%

From the table above, we can see that the diagnostic accuracy is excellent at 900 rpm high speed regardless of whether characteristic parameters or the principal components of the characteristic parameters is used. However, at lower speeds, the diagnostic accuracy is not ideal, it is difficult to meet the needs of precision diagnosis.

5.6.4 The summary of result of each method based on neural networks

In order to more easily compare the diagnostic accuracy of each method, the diagnostic results of the methods mentioned in this study are summarized in a table as follows:

Table. 12 The summary of result of each method based on neural networks

Diagnosis method	The type of diagnostic data	Rotating speed	Diagnostic accuracy
Back propagation neural network	Symptom parameters	300rpm	16%
Back propagation neural network	Symptom parameters	500rpm	16%
Back propagation neural network	Symptom parameters	700rpm	23%
Back propagation neural network	Symptom parameters	900rpm	18%
Back propagation neural network	Principal component	300rpm	17%
Back propagation neural network	Principal component	500rpm	11%
Back propagation neural network	Principal component	700rpm	16%
Back propagation neural network	Principal component	900rpm	12%
Convolutional neural network	Symptom parameters	300rpm	70%
Convolutional neural network	Symptom parameters	500rpm	70%
Convolutional neural network	Symptom parameters	700rpm	80%
Convolutional neural network	Symptom parameters	900rpm	99%
Convolutional neural network	Principal component	300rpm	70%
Convolutional neural network	Principal component	500rpm	80%
Convolutional neural network	Principal component	700rpm	80%
Convolutional neural network	Principal component	900rpm	99%
Deep belief neural network	Time domain signal	300rpm	20%

Deep belief neural network	Time domain signal	500rpm	20%
Deep belief neural network	Time domain signal	700rpm	20%
Deep belief neural network	Time domain signal	900rpm	20%
Deep belief neural network	Frequency domain signal	300rpm	80%
Deep belief neural network	Frequency domain signal	500rpm	82%
Deep belief neural network	Frequency domain signal	700rpm	98%
Deep belief neural network	Frequency domain signal	900rpm	96%
Deep belief neural network	Frequency domain signal after extracting fault features	300rpm	100%
Deep belief neural network	Frequency domain signal after extracting fault features	500rpm	100%
Deep belief neural network	Frequency domain signal after extracting fault features	700rpm	99%
Deep belief neural network	Frequency domain signal after extracting fault features	900rpm	100%

5.7 Summary

In this study, to realize accurate detection and recognition of structural faults of rotating machinery, a precise diagnosis method based on fault information extraction that combines EMD and sample entropy as well as DBN was proposed. Diagnosis results based on time-domain signals, diagnosis results based on frequency-domain signals, and diagnosis results based on the combination of frequency-domain signals and fault information were compared. It finds that diagnosis accuracy based on time-domain signals was unsatisfying, because time-domain signals are difficult to express all features of signals, so fail to detect and recognize structural faults. The most prominent common features of structural faults are changes of rotating frequency and its harmonic components. Therefore, diagnosis accuracy based on frequency-domain signals was increased significantly compared with that based on time-domain signals. Since different types of structural faults have similar features in the frequency domain, the diagnosis accuracy based on frequency-domain signals under low rotating speed is unsatisfying and has to be improved. When fault information was extracted by combining EMD and sample entropy, the original vibration signals were decomposed

and signals with high SNR that contain abundant fault characteristics were selected and reconstructed into new vibration signals. Frequency-domain signals of these new vibration signals were used in diagnosis, which achieves high accuracy under both high and low rotating speeds. In other words, the proposed method can detect and recognize structural faults under different rotating speeds. It realizes precise diagnosis of structural faults. Moreover, an intelligent precise diagnosis system can be constructed based on the propose method. This is conducive to realize the goal of early diagnosis of structural faults in practical production. Compared with BPNN and CNN, the method proposed in this study was superior to other methods in the precision diagnosis of structural faults in rotating machinery, and has the highest diagnostic accuracy.

6. Conclusions

In the first half of the research, the dynamic models of axial vibration of shaft misalignment state were proposed. In order to obtain the solution of the dynamic models and clarify the feature of the vibration signal in misalignment states, we showed the method to calculate the vibration displacement caused by each misalignment state. The computer simulation and experiment using rotating machine were also shown to verify the efficiency of the dynamic analysis method proposed in this paper.

The subsequent research has realized the integration of vibration acceleration signals measured at multiple positions and multiple directions based on the structural feature symptom parameters, and proposed the method to diagnose the structural faults of rotating machinery (misalignment state, unbalanced state and loosening state) based on successive multivariate analysis. This method can realize the detection of structural faults of rotating machinery and the identification of types of anomalies. The validity of this methodology was confirmed by the experiment with the rotating machine simulator.

Finally, we propose and compare several diagnostic methods for structure faults based on neural network. Although BP neural network is advantageous in pattern recognition and the input special characteristic parameters have extracted features of the original signals, the diagnosis based on BP neural network is still unsatisfying and far from precise diagnosis. This is because signals of structural abnormalities are complicated and the BP neural network is too simple to learn all fault characteristics.

Since deep CNN has complicated deep structures and can extract and learn more fault characteristics from signals, diagnosis method based on deep CNN achieves significantly higher accuracy than that based on BP neural network. However, due to complexity of structural abnormalities in low-frequency domain, deep CNN still fails to extract adequate low-frequency features to increase the diagnosis accuracy. Hence, the diagnosis accuracy based on deep CNN under low rotating speed cannot meet requirements of precise diagnosis.

To realize accurate detection and recognition of structural abnormalities of rotating machinery, a precise diagnosis method based on fault information extraction that combines EMD and sample entropy as well as DBN is proposed. Diagnosis results based on time-domain signals, diagnosis results based on frequency-domain signals, and diagnosis results based on the combination of frequency-domain signals and fault information are compared. It finds that diagnosis accuracy based on time-domain

signals is unsatisfying, because time-domain signals are difficult to express all features of signals. It fails to detect and recognize structural abnormalities. The most prominent common features of structural abnormalities are changes of rotating frequency and its harmonic components. Therefore, diagnosis accuracy based on frequency-domain signals is increased significantly compared with that based on time-domain signals. Since different types of structural abnormalities have similar features in the frequency domain, the diagnosis accuracy based on frequency-domain signals under low rotating speed is unsatisfying and has to be improved. When fault information is extracted by combining EMD and sample entropy, the original vibration signals are decomposed and signals with high SNR that contain abundant fault characteristics are selected and reconstructed into new vibration signals. Frequency-domain signals of these new vibration signals are used in diagnosis, which achieves high accuracy under both high and low rotating speeds. In other words, the proposed method can detect and recognize structural abnormalities under different rotating speeds. It realizes precise diagnosis of structural abnormalities. Moreover, an intelligent precise diagnosis system can be constructed based on the propose method. This is conducive to realize the goal of early diagnosis of structural abnormalities in practical production.

References

[1] Yaguo Lei, Jing Lin, Zhengjia He, Ming J. Zuo, A review on empirical mode decomposition in fault diagnosis of rotating machinery, Mechanical Systems and Signal Processing **2013**, 35, (1–2), 108–126.

[2] Zhinong Li, Zhaotong Wu, Yongyong He, Chu Fulei, Hidden Markov model-based fault diagnostics method in speed-up and speed-down process for rotating machinery, Mechanical Systems and Signal Processing **2005**, 19, (2), 329–339.

[3] Tejas H. Patela, Ashish K. Darpe, Experimental investigations on vibration response of misaligned rotors, Mechanical Systems and Signal Processing **2009**, 23, (7), 2236–2252.

[4] Li, B., Mo-Yuen Chow, Tipsuwan Y., Hung J.C., Neural-network-based motor rolling bearing fault diagnosis, IEEE transactions on industrial electronics **2000**, 47, (5), 1060 -1069.

[5] Robert B. Randall, State of the Art in Monitoring Rotating Machinery – Part 1, Sound and vibration **2004**, 38, (3), 14-21.

[6] Arun Kr. Jalan A.R. Mohanty, Model based fault diagnosis of a rotor–bearing system for misalignment and unbalance under steady-state condition, Journal of Sound and Vibration **2009**, 327, (3-5), 604–622.

[7] Finley W.R., Hodowanec M.M., Holter, W.G, An analytical approach to solving motor vibration problems, Industry Applications Society 46th Annual Petroleum and Chemical Technical Conference (Cat. No. 99CH37000). IEEE **1999**, 217-232.

[8] Aiwina Heng, Sheng Zhang, Andy C.C. Tan, Joseph Mathew, Rotating machinery prognostics: State of the art, challenges and opportunities, Mechanical Systems and Signal Processing **2009**, 23, (3), 724–739.

[9] P. Pennacchi and A. Vania, Diagnosis and model based identification of a coupling misalignment, Shock and Vibration **2005**, 12, (4), 293–308.

[10] P N Saavedra and D E Ramírez, Vibration analysis of rotors for the identification of shaft misalignment Part 2: Experimental validation, Proceedings of the Institution of Mechanical Engineers, Part C: Journal of Mechanical Engineering Science **2004**, 218, (9), 987-999.

[11] Chen, Peng, Toshio Toyota, and Zhengja He, Automated function generation of symptom parameters and application to fault diagnosis of machinery under variable operating conditions, IEEE Transactions on systems, man, and cybernetics-Part A:

Systems and Humans **2001**, 31, (6), 775-781.

[12] Li, Bo, M-Y. Chow, Yodyium Tipsuwan, and James C. Hung, Neural-network-based motor rolling bearing fault diagnosis, IEEE transactions on industrial electronics **2000**, 47, (5), 1060-1069.

[13] Bishop, Christopher M., Neural networks for pattern recognition: Oxford University Press, New York 1996.

[14] Samanta, B., and K. R. Al-Balushi, Artificial neural network based fault diagnostics of rolling element bearings using time-domain features, Mechanical systems and signal processing **2003**, 17, (2), 317-328.

[15] Radzieński, Maciej, Marek Krawczuk, and Magdalena Palacz. Improvement of damage detection methods based on experimental modal parameters, Mechanical Systems and Signal Processing **2011**, 25, (6), 2169-2190.

[16] Chen, Peng, Toshio Toyota, and Zhengja He, Automated function generation of symptom parameters and application to fault diagnosis of machinery under variable operating conditions, IEEE Transactions on systems, man, and cybernetics-Part A: Systems and Humans **2001**, 31, (6), 775-781.

[17] Li, Bo, M-Y. Chow, Yodyium Tipsuwan, and James C. Hung, Neural-network-based motor rolling bearing fault diagnosis, IEEE transactions on industrial electronics **2000**, 47, (5), 1060-1069.

[18] Götz, Oliver, Kerstin Liehr-Gobbers, and Manfred Krafft, Evaluation of structural equation models using the partial least squares (PLS) approach, In Handbook of partial least squares 2010, 691-711.

[19] Randall, R. B.; Antoni, J., Rolling element bearing diagnostics—A tutorial, Mechanical systems and signal processing 2011, 25, (2), 485-520.

[20] Xue, H.; Wang, H.; Chen, P.; Li, K.; Song, L., Automatic diagnosis method for structural fault of rotating machinery based on distinctive frequency components and support vector machines under varied operating conditions, Neurocomputing 2013, 116, 326-335.

[21] Chen, P.; Toyota, T.; He, Z., Automated function generation of symptom parameters and application to fault diagnosis of machinery under variable operating conditions, IEEE Transactions on systems, man, and cybernetics-Part A: Systems and Humans 2001, 31, (6), 775-781.

[22] Wang, X.; Zheng, Y.; Zhao, Z.; Wang, J., Bearing fault diagnosis based on statistical locally linear embedding, Sensors 2015, 15, (7), 16225-16247.

[23] Bishop, C. M., Neural networks for pattern recognition, Oxford university press 1995.

[24] Xia, Z.; Xia, S.; Wan, L.; Cai, S., Spectral regression based fault feature extraction for bearing accelerometer sensor signals, Sensors 2012, 12, (10), 13694-13719.

[25] Lei, Y.; He, Z.; Zi, Y.; Chen, X., New clustering algorithm-based fault diagnosis using compensation distance evaluation technique, Mechanical Systems and Signal Processing 2008, 22, (2), 419-435.

[26] Mojiri, M.; Karimi-Ghartemani, M.; Bakhshai, A., Time-domain signal analysis using adaptive notch filter, IEEE Transactions on Signal Processing 2007, 55, (1), 85-93.

[27] Shynk, J. J., Frequency-domain and multirate adaptive filtering, IEEE Signal Processing Magazine 1992, 9, (1), 14-37.

[28] Zhao, M.; Lin, J.; Xu, X.; Lei, Y., Tacholess envelope order analysis and its application to fault detection of rolling element bearings with varying speeds, Sensors 2013, 13, (8), 10856-10875.

[29] Widodo, A.; Kim, E. Y.; Son, J.-D.; Yang, B.-S.; Tan, A. C.; Gu, D.-S.; Choi, B.-K.; Mathew, J., Fault diagnosis of low speed bearing based on relevance vector machine and support vector machine, Expert systems with applications 2009, 36, (3), 7252-7261.

[30] Meltzer, G.; Dien, N. P., Fault diagnosis in gears operating under non-stationary rotational speed using polar wavelet amplitude maps, Mechanical Systems and Signal Processing 2004, 18, (5), 985-992.

[31] Cempel, C.; Tabaszewski, M., Multidimensional condition monitoring of machines in non-stationary operation, Mechanical Systems and Signal Processing 2007, 21, (3), 1233-1241.

[32] Lei, Y.; Li, N.; Lin, J.; Wang, S., Fault diagnosis of rotating machinery based on an adaptive ensemble empirical mode decomposition, Sensors 2013, 13, (12), 16950-16964

[33] Huang, N. E.; Shen, Z.; Long, S. R.; Wu, M. C.; Shih, H. H.; Zheng, Q.; Yen, N.-C.; Tung, C. C.; Liu, H. H. In The empirical mode decomposition and the Hilbert spectrum for nonlinear and non-stationary time series analysis, Proceedings of the Royal Society of London A: mathematical, physical and engineering sciences, 1998; The Royal Society: 1998; pp 903-995.

[34] Peng, Z.; Peter, W. T.; Chu, F., A comparison study of improved Hilbert–Huang transform and wavelet transform: application to fault diagnosis for rolling bearing, Mechanical systems and signal processing 2005, 19, (5), 974-988.

[35] Lei, Y.; Lin, J.; He, Z.; Zuo, M. J., A review on empirical mode decomposition in fault diagnosis of rotating machinery, Mechanical systems and signal processing 2013, 35, (1-2), 108-126.

[36] Chow, M.-Y.; Chew, A. V.; Yee, S.-O. In Performance of a fault detector artificial neural network using different paradigms, Applications of Artificial Neural Networks III, 1992; International Society for Optics and Photonics: 1992; pp 973-982.

[37] Li, B.; Goddu, G.; Chow, M.-Y. In Detection of common motor bearing faults using frequency-domain vibration signals and a neural network based approach, American Control Conference, 1998. Proceedings of the 1998, 1998; IEEE: 1998; pp 2032-2036.

[38] Zhu, L.; Chen, L.; Zhao, D.; Zhou, J.; Zhang, W., Emotion recognition from chinese speech for smart affective services using a combination of SVM and DBN, Sensors 2017, 17, (7), 1694.

[39] Lv, Q.; Dou, Y.; Niu, X.; Xu, J.; Xu, J.; Xia, F., Urban land use and land cover classification using remotely sensed SAR data through deep belief networks, Journal of Sensors 2015, 2015.

[40] Li, C.; Sánchez, R.-V.; Zurita, G.; Cerrada, M.; Cabrera, D., Fault diagnosis for rotating machinery using vibration measurement deep statistical feature learning, Sensors 2016, 16, (6), 895.

[41] He, J.; Yang, S.; Gan, C., Unsupervised fault diagnosis of a gear transmission chain using a deep belief network, Sensors 2017, 17, (7), 1564.

[42] LeCun, Y.; Bengio, Y.; Hinton, G., Deep learning, nature 2015, 521, (7553), 436.

[43] Xie, J.; Du, G.; Shen, C.; Chen, N.; Chen, L.; Zhu, Z., An End-to-End Model Based on Improved Adaptive Deep Belief Network and Its Application to Bearing Fault Diagnosis, IEEE Access 2018.

[44] Hinton, G. E.; Osindero, S.; Teh, Y.-W., A fast learning algorithm for deep belief nets, Neural computation 2006, 18, (7), 1527-1554.

[45] Hinton, G. E., A practical guide to training restricted Boltzmann machines, In Neural networks: Tricks of the trade, Springer: 2012; pp 599-619.

[46] Cempel, C., Implementing multidimensional inference capability in vibration

condition monitoring, Diagnostyka 2005, 34, 7-14

[47] Wang, H.; Chen, P., A feature extraction method based on information theory for fault diagnosis of reciprocating machinery, Sensors 2009, 9, (4), 2415-2436.

[48] Li, K.; Zhang, Q.; Wang, K.; Chen, P.; Wang, H., Intelligent condition diagnosis method based on adaptive statistic test filter and diagnostic bayesian network, Sensors 2016, 16, (1), 76.

[49] Buscema, M., Back propagation neural networks, Substance use & misuse 1998, 33, (2), 233-270.

[50] Krizhevsky, A.; Sutskever, I.; Hinton, G. E. In Imagenet classification with deep convolutional neural networks, Advances in neural information processing systems 2012, 1097-1105.